

A SIMPLE HYPOPLASTIC CONSTITUTIVE MODEL FOR SAND

WEI WU

Lahmeyer International Ltd., 60528 Frankfurt, Germany

AND

ERICH BAUER

Institute of Mechanics, Technical University of Graz, 8010 Graz, Austria

SUMMARY

The paper presents a hypoplastic constitutive model for the three-dimensional non-linear stress–strain and dilatant volume change behaviour of sand. The model is developed without recourse to the concept in elastoplasticity theory such as yield surface, plastic potential and decomposition into elastic and plastic parts. Benefited from the non-linear tensorial functions available from the representation theorem the model possesses simple mathematical formulation and contains only four material parameters, which can be easily identified with triaxial compression tests. Comparison of the predictions with the experimental results shows that the model is capable of capturing the salient behaviour of sand under monotonic loading and is applicable to both drained and undrained conditions.

1. INTRODUCTION

Following the pioneer Cam-clay model developed by the Cambridge soil mechanics school,¹ much effort has been devoted to the development of constitutive models that are capable of predicting the mechanical behaviour of soils. The varying emphasis on describing different aspects of the behaviour of soils has given rise to a large number of models with different levels of sophistication and complexity. The capability of the models has been greatly enhanced by introducing various concepts such as the double yield surfaces,² the bounding surface,³ the anisotropic hardening rule⁴ and the endochronic intrinsic time.⁵

When the various models proposed in the past are examined, it is evident that the capacity of the models has been gained at the cost of their simplicity. Along with the sophistication of the models, more complicated mathematical formulations have been adduced and the number of the material parameters has also increased considerably. However, complex mathematical relations have rendered a clear insight into the models impossible, and the identification of the many parameters has been proved to be more than difficult. The question arises whether such complex formulations can be justified, particularly in view of the fact that soils are natural products and usually show large variation in their property. The Cam-clay model provides an answer to the above question, since the model captures the salient features of normally consolidated clays with only three easily measurable material parameters. From the practical point of view, a constitutive model capable of reproducing the essential features, although not all facets, of the material behaviour with simpler mathematical formulations and fewer material parameters is to be favoured.

A perusal of the relevant literature also reveals that while there exist several well-established, relatively simple constitutive models for clay, comparably simple models for sand are still lacking. This situation is mainly due to the more complex behaviour of sand as compared with clay. Whereas the volume change of loose and is contractant throughout, dense sand shows an initial contractancy and a subsequent dilatancy. As a consequence, the associated flow rule in elastoplasticity does not apply. Liquefaction and cyclic mobility mark further characteristics that are substantially different from that of clay. The existing models for sand are often rather complicated in their formulations and usually involve many material parameters.

Our primary purpose is to develop a constitutive model that is capable of capturing the salient behaviour of sand and is yet as simple as the Cam-clay model. In developing such a constitutive model, an ensuing question is whether we should follow the elastoplastic theory or we had better tread a radically new way. It seems that the various modifications of the existing elastoplastic models lead inevitably to rather involved formulations. In fact, it is a common phenomenon in the development of science that a simple model, e.g. the Cam-clay model, which is originally proposed to describe the salient features of the observations, fails to account for more refined experiments. Modifications are then included to describe the new observations. This process of modifications will continue until the model becomes too complicated to be applied. A new theory with simpler mathematical formulation and fewer material parameters is bound to emerge. We believe that this new theory cannot be achieved through modifications to the existing elastoplastic model. To quote from Roscoe:⁶ "I have always rejected the idea that the best way to make progress is continually to apply small modifications to current methods."

Based on the non-linear tensorial functions, a hypoplastic model is developed as an alternative approach to the prevailing elastoplastic models in describing the mechanical behaviour of sands. The corner-stones pertinent to elastoplasticity such as yield surface, plastic potential, decomposition of the deformation into elastic and plastic parts, hardening and flow rule are abandoned to be used in formulating the constitutive model. In this way, a constitutive model with elegant mathematical formulation and with only four material parameters is achieved. It is shown that many well-established concepts in soil mechanics can be unified with the constitutive model, and failure surface, flow rule and the earth pressure coefficient at rest, which have to be prescribed *a priori* in most elastoplastic models, now turn out as natural outcomes of the constitutive model.

Our previous publications have been addressed mainly to researchers in continuum mechanics.⁷⁻¹³ The present paper is an attempt to communicate with geotechnical engineers. To skirt the difficulties of engineers with tensorial calculations, second-rank matrices are used. To make the constitutive model more comprehensive, explicit expressions for simulating the laboratory tests are provided where necessary. Special emphasis is placed on the identification of the material parameters in the model through correlation with some widely used parameters in soil mechanics.

2. FRAMEWORK OF HYPOPLASTICITY

Let the motion of a granular body be referred to some fixed rectangular Cartesian co-ordinates and let the granular body occupy the position \mathbf{X} in some reference configuration. Suppose the motion of the granular media can be described by $\mathbf{x} = \mathbf{x}(\mathbf{X}, t)$.

The following dynamic and kinematic quantities are used in formulating the constitutive equation: the Cauchy stress tensor $\boldsymbol{\sigma}$, the strain rate and spin tensors, $\dot{\boldsymbol{\epsilon}}$ and $\dot{\boldsymbol{\omega}}$. The strain rate and spin tensors are related to the velocity gradient as follows:

$$\dot{\boldsymbol{\epsilon}} = \frac{1}{2}[(\nabla\dot{\mathbf{x}}) + (\nabla\dot{\mathbf{x}})^T], \quad \dot{\boldsymbol{\omega}} = \frac{1}{2}[(\nabla\dot{\mathbf{x}}) - (\nabla\dot{\mathbf{x}})^T] \quad (1)$$

where ∇ stands for the gradient and the superscript T denotes a transposition. Throughout the paper, we will use bold letters to denote tensors and matrices. A superposed dot implies material time differentiation. To comply with the sign convention in soil mechanics tensile stress, elongative strain and their rate are taken to be negative.

2.1. Hypoplastic constitutive equation

Following the recent work by Wu and Kolymbas,⁸ we define our hypoplastic constitutive model by assuming that there exists a tensorial function \mathbf{H} such that

$$\dot{\boldsymbol{\sigma}} = \mathbf{H}(\boldsymbol{\sigma}, \dot{\boldsymbol{\varepsilon}}) \quad (2)$$

where $\dot{\boldsymbol{\sigma}}$ is the Jaumann stress rate defined as follows:

$$\dot{\boldsymbol{\sigma}} = \dot{\boldsymbol{\sigma}} + \boldsymbol{\sigma}\dot{\boldsymbol{\omega}} - \dot{\boldsymbol{\omega}}\boldsymbol{\sigma} \quad (3)$$

Furthermore, we require that the function \mathbf{H} in (2) is not differentiable in and only in $\dot{\boldsymbol{\varepsilon}} = \mathbf{0}$.

It should be remarked that by virtue of constitutive equation (2), the stress rate depends solely on the instantaneous stress state and is independent of the way in which this stress state is reached. Note that the above remark is only valid for the instantaneous behaviour. The overall behaviour predicted by (2) depends in general on the stress path.

By virtue of relation (2), the history dependence of the constitutive model is reduced to the instantaneous stress. It is certainly true that the history dependence in general might be more complex. We will, however, consider (2) as a reasonable assumption to get a simple formulation. The non-differentiability of \mathbf{H} at $\dot{\boldsymbol{\varepsilon}} = \mathbf{0}$ means that the hypoplastic constitutive model is necessarily incrementally non-linear. Recalling the hypoelastic constitutive equation proposed by Truesdell,¹⁴ it can be seen that our definition of hypoplasticity is furnished by requiring that \mathbf{H} is not differentiable at $\dot{\boldsymbol{\varepsilon}} = \mathbf{0}$. As we know, irreversible deformation cannot be described within the framework of hypoelasticity. The non-differentiability of \mathbf{H} in $\dot{\boldsymbol{\varepsilon}}$ is therefore a decisive step towards taking the irreversible behaviour into consideration. Consider a constitutive equation $\dot{\boldsymbol{\sigma}} = \mathbf{H}(\boldsymbol{\sigma}, \dot{\boldsymbol{\varepsilon}})$ and a closed strain cycle by applying $\dot{\boldsymbol{\varepsilon}}$ and $-\dot{\boldsymbol{\varepsilon}}$ sequentially. If the constitutive equation in concern is differentiable at $\dot{\boldsymbol{\varepsilon}} = \mathbf{0}$, we obtain the same tangential stiffness for both $\dot{\boldsymbol{\varepsilon}}$ and $-\dot{\boldsymbol{\varepsilon}}$, i.e. $\lim_{D \rightarrow 0^+} \partial \mathbf{H} / \partial \dot{\boldsymbol{\varepsilon}} = \lim_{D \rightarrow 0^-} \partial \mathbf{H} / \partial \dot{\boldsymbol{\varepsilon}}$. Apparently, the resultant stress after the strain cycle will be zero. As a consequence, the dissipative behaviour cannot be accounted for. If, however, the constitutive equation is not differentiable at $\dot{\boldsymbol{\varepsilon}} = \mathbf{0}$, the tangential stiffness and therefore the stress rate for $\dot{\boldsymbol{\varepsilon}}$ and $-\dot{\boldsymbol{\varepsilon}}$ will be in general different giving rise to the desired dissipative behaviour. For comparison, the non-differentiability in an elastoplastic model is achieved by using different relations for loading and unloading, whereas a single relation is used in the hypoplastic model.

We seek to obtain a concrete formulation by imposing several restrictions on constitutive equation (2). Some of these restrictions are based on the general principles of continuum mechanics, while others are based on experimental observations. Assume that the behaviour to be described is rate-independent. In this case, no material parameter with the dimension of time can enter the constitutive equation.¹⁵ For constitutive equation (2), rate-independence is equivalent to the following statement.

Restriction 1: The function \mathbf{H} should be positively homogeneous of the first order in $\dot{\boldsymbol{\varepsilon}}$:

$$\mathbf{H}(\boldsymbol{\sigma}, \lambda \dot{\boldsymbol{\varepsilon}}) = \lambda \mathbf{H}(\boldsymbol{\sigma}, \dot{\boldsymbol{\varepsilon}}) \quad (4)$$

where λ is a positive but otherwise arbitrary scalar.

The second restriction results from the requirement of objectivity.¹⁶ The material response, as described by constitutive equation (2), should remain invariant under rigid rotations.

Restriction 2: The function \mathbf{H} should fulfil the following condition of objectivity:

$$\mathbf{H}(\mathbf{Q}\boldsymbol{\sigma}\mathbf{Q}^T, \mathbf{Q}\dot{\boldsymbol{\varepsilon}}\mathbf{Q}^T) = \mathbf{Q}\mathbf{H}(\boldsymbol{\sigma}, \dot{\boldsymbol{\varepsilon}})\mathbf{Q}^T \quad (5)$$

is which \mathbf{Q} is an orthogonal tensor.

The requirement of objectivity is satisfied if the function \mathbf{H} is chosen according to the representation theorems for isotropic tensorial functions. In the most general case, the representation theorem for a tensorial function of two symmetric tensors can be written as¹⁷

$$\begin{aligned} \dot{\boldsymbol{\sigma}} = & \alpha_0 \mathbf{1} + \alpha_1 \boldsymbol{\sigma} + \alpha_2 \dot{\boldsymbol{\varepsilon}} + \alpha_3 \boldsymbol{\sigma}^2 + \alpha_4 \dot{\boldsymbol{\varepsilon}}^2 + \alpha_5 (\boldsymbol{\sigma} \dot{\boldsymbol{\varepsilon}} + \dot{\boldsymbol{\varepsilon}} \boldsymbol{\sigma}) \\ & + \alpha_6 (\boldsymbol{\sigma}^2 \dot{\boldsymbol{\varepsilon}} + \dot{\boldsymbol{\varepsilon}} \boldsymbol{\sigma}^2) + \alpha_7 (\boldsymbol{\sigma} \dot{\boldsymbol{\varepsilon}}^2 + \dot{\boldsymbol{\varepsilon}}^2 \boldsymbol{\sigma}) + \alpha_8 (\boldsymbol{\sigma}^2 \dot{\boldsymbol{\varepsilon}}^2 + \dot{\boldsymbol{\varepsilon}}^2 \boldsymbol{\sigma}^2) \end{aligned} \quad (6)$$

where $\mathbf{1}$ is the unit tensor. The coefficients in (6), α_i ($i = 0, \dots, 8$) are functions of the invariants and joint invariants of $\boldsymbol{\sigma}$ and $\dot{\boldsymbol{\varepsilon}}$:

$$\alpha_i = \alpha_i(\text{tr } \boldsymbol{\sigma}, \text{tr } \boldsymbol{\sigma}^2, \text{tr } \boldsymbol{\sigma}^3, \text{tr } \dot{\boldsymbol{\varepsilon}}, \text{tr } \dot{\boldsymbol{\varepsilon}}^2, \text{tr } \dot{\boldsymbol{\varepsilon}}^3, \text{tr } (\boldsymbol{\sigma} \dot{\boldsymbol{\varepsilon}}), \text{tr } (\boldsymbol{\sigma}^2 \dot{\boldsymbol{\varepsilon}}), \text{tr } (\boldsymbol{\sigma} \dot{\boldsymbol{\varepsilon}}^2), \text{tr } (\boldsymbol{\sigma}^2 \dot{\boldsymbol{\varepsilon}}^3)) \quad (7)$$

where tr represents the trace of a tensor. Note that the isotropy of the tensorial function does not necessarily mean that the response is also isotropic. In fact, anisotropy due to variation of stress can be accounted for.

The third restriction is based on the following experimental observation made by Golscheider¹⁸ with a true triaxial apparatus on sand:

A proportional strain (stress) path starting from a nearly stress free and undistorted state yields a proportional stress (strain) path.

This observation is of fundamental importance for developing constitutive equations. Mathematically, it can be expressed by the following restriction.

Restriction 3: The function \mathbf{H} should be homogeneous in $\boldsymbol{\sigma}$, i.e.

$$\mathbf{H}(\lambda \boldsymbol{\sigma}, \dot{\boldsymbol{\varepsilon}}) = \lambda^n \mathbf{H}(\boldsymbol{\sigma}, \dot{\boldsymbol{\varepsilon}}) \quad (8)$$

where λ is an arbitrary scalar and n denotes the order of homogeneity. Restriction 3 implies that the tangential stiffness is proportional to the n th power of the stress level $(\text{tr } \boldsymbol{\sigma})^n$, so that experiments conducted under different stress levels can be normalized by $(\text{tr } \boldsymbol{\sigma})^n$. This so-called normalized behaviour for granular materials has been widely reported in the literature.¹⁹

2.2. A subclass of hypoplastic constitutive equations

Without loss in generality, we confine ourselves to constitutive equations of the tensor generators from the representation theorem (6) and assume further that the constitutive equation can be decomposed into two parts representing reversible and irreversible behaviour of the material:

$$\dot{\boldsymbol{\sigma}} = \mathbf{L}(\boldsymbol{\sigma}, \dot{\boldsymbol{\varepsilon}}) - \mathbf{N}(\boldsymbol{\sigma}, \dot{\boldsymbol{\varepsilon}}) \quad (9)$$

where \mathbf{L} is assumed to be linear in $\dot{\boldsymbol{\varepsilon}}$ and \mathbf{N} is non-linear in $\dot{\boldsymbol{\varepsilon}}$. It is worthwhile to notice that if we drop $\mathbf{N}(\boldsymbol{\sigma}, \dot{\boldsymbol{\varepsilon}})$ in (9), then the hypoelastic constitutive equation due to Truesdell¹⁴ is recovered. In this sense, hypoplastic constitutive equations can also be regarded as an extension of the hypoelastic constitutive equation. Application of hypoelasticity to granular materials has been

attempted by Stutz,²⁰ Romano²¹ and Davis and Mullenger.²² Several critiques on the hypoelastic models for soils can be found in the work by Gudehus.²³ In particular, the response of such constitutive models may show jumps for certain directions of strain rate.

$\mathbf{L}(\boldsymbol{\sigma}, \dot{\boldsymbol{\varepsilon}})$ in (9) can be specified by invoking the representation theorem for isotropic tensorial functions. Keeping in mind that the non-linear dependence on \mathbf{N} on $\dot{\boldsymbol{\varepsilon}}$ should also satisfy the restriction of rate-independence, we consider the following constitutive equation:

$$\dot{\boldsymbol{\sigma}} = \mathbf{L}(\boldsymbol{\sigma}) : \dot{\boldsymbol{\varepsilon}} - \mathbf{N}(\boldsymbol{\sigma}) \|\dot{\boldsymbol{\varepsilon}}\| \quad \text{Of} \quad (10)$$

where $\mathbf{L} = \partial \mathbf{L} / \partial \dot{\boldsymbol{\varepsilon}}$ is, in analogy to the elastic stiffness matrix, a fourth-order tensor and $\|\dot{\boldsymbol{\varepsilon}}\| = \sqrt{\text{tr } \dot{\boldsymbol{\varepsilon}}^2}$ stands for the Euclidean norm. The colon : denotes an inner product between two tensors. Without inducing confusion the same symbol \mathbf{N} is retained in (10). The concrete form of \mathbf{N} can also be obtained with the help of the representation theorem for isotropic tensorial functions. Due to the non-differentiable term containing $\|\dot{\boldsymbol{\varepsilon}}\|$, constitutive equation (10) is incrementally non-linear. Constitutive equation (10) defines a class of hypoplastic constitutive equations, which can be used to describe the behaviour of granular materials.

Note that the concepts in elastoplastic theory such as yield surface, plastic potential and decomposition of deformation into elastic and plastic parts are not used in developing the constitutive model. There is even no need to define loading and unloading explicitly, since they are implied by the constitutive equation. To show how loading and unloading can be accounted for by (10) and to bring out the relationship between hypoplastic and elastoplastic models, let us consider the case of one-dimensional stress and strain and apply two strain rates of the same magnitude and in opposite directions, $\dot{\varepsilon}$ (loading) and $-\dot{\varepsilon}$ (unloading). The following equations are obtained by substituting $\dot{\varepsilon}$ and $-\dot{\varepsilon}$ into (10):

$$\dot{\sigma} = \begin{cases} [L - N] \dot{\varepsilon} & \dot{\varepsilon} > 0 \\ [L + N] \dot{\varepsilon} & \dot{\varepsilon} < 0 \end{cases} \quad (11)$$

The terms in the brackets in (11) represent the tangential stiffness. As can be seen from the above equations, two distinct stiffnesses are obtained for loading and unloading.

The relationship between hypoplastic and elastoplastic models will become apparent by comparing the stiffnesses in (11) to the stiffnesses in an elastoplastic model:

$$\dot{\sigma} = \begin{cases} L^{\text{ep}} : \dot{\varepsilon} & \dot{\varepsilon} > 0 \\ L^{\text{ec}} : \dot{\varepsilon} & \dot{\varepsilon} < 0 \end{cases} \quad (12)$$

where L^{ep} and L^{ec} denote the elastoplastic and the elastic stiffness, respectively. The following relations can be easily seen by comparing (11) with (12):

$$\begin{aligned} L - N &= L^{\text{ep}} \\ L + N &= L^{\text{ec}} \end{aligned} \quad (13)$$

It should be reminded that the relations in (13) are merely formal, since the stiffness predicted by a hypoplastic model need not be identical with that by an elastoplastic model. Furthermore, the one-dimensional models in (11) and (12) are certainly oversimplified for the three-dimensional behaviour, since stress, strain and their rates are tensorial quantities.

The underlying difference between hypoplastic and elastoplastic models can be further demonstrated with the help of the stress-strain curves in Figure 1. We first consider the elastoplastic model as specified by (12) and rewrite the constitutive equation for loading as follows: $\dot{\sigma} = L^{\text{ec}}(\dot{\varepsilon} - \dot{\varepsilon}^{\text{p}}) = L^{\text{ec}}\dot{\varepsilon} - L^{\text{ec}}\dot{\varepsilon}^{\text{p}}$ with $\dot{\varepsilon}^{\text{p}}$ being the plastic strain rate. To calculate the stress rate upon loading, $\dot{\sigma} \Delta t$ (c in Figure 1(a)), one can first compute the stress rate, which results from the

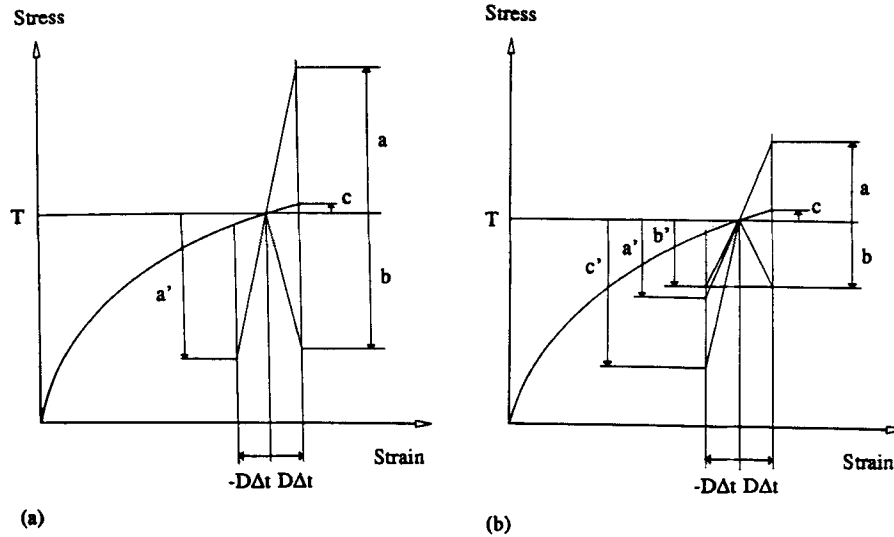


Figure 1. Schematic interpretation of constitutive equation (10)

elastoplastic constitutive model

total strain rate $L^{ee}\dot{\epsilon}$ (a in Figure 1(a)), and then subtract the amount $L^{ee}\dot{\epsilon}^p$ on account of the plastic effect (b in Figure 1(a)), i.e. $c = a - b$. For unloading, $-\dot{\epsilon}\Delta t$, the stress rate, a' in Figure 1(a), is calculated elastically from the total strain rate. It is clear from Figure 1(a) that $a = -a'$.

Next, the hypoplastic constitutive model as given by (11) is considered. The stress rate upon loading, c in Figure 1(b), can be calculated as the difference between the stress rate resulting from the linear term $L\dot{\epsilon}$ (a in Figure 1(b)) and the stress rate from the non-linear term $N\dot{\epsilon}$ (b in Figure 1(b)), i.e. $c = a - b$ in Figure 1(b). For unloading, however, the behavior of a hypoplastic model differs substantially from an elastoplastic model. The behavior upon unloading is not assumed to be purely elastic. Rather, the stress rate is the sum of the stress rates resulting from the linear and the non-linear terms, i.e. $c' = a' + b'$ in Figure 1(b). From Figure 1(b) we have $a = -a'$ and $b = b'$. On unloading, the stress rate from the elastoplastic model in Figure 1(a) can be regarded as a special case of the hypoplastic model in Figure 1(b) with $b' = 0$.

To show the difference between hypoplasticity and elastoplasticity in more detail, constitutive equation (10) can be recast in a more convenient form by virtue of Euler's theorem for homogeneous functions:

$$\dot{\sigma} = (L - N \otimes \bar{\dot{\epsilon}}) : \dot{\epsilon}, \quad (14)$$

in which $\bar{\dot{\epsilon}} = \dot{\epsilon}/\|\dot{\epsilon}\|$ stands for the direction of strain rate. The symbol \otimes denotes an outer product between two tensors.

The two terms in the brackets in (14) represent the tangential stiffness tensor. It is apparent from (14) that the tangential stiffness tensor depends not only on stress but also on the direction of strain rate. As compared with elastoplasticity theory, hypoplastic constitutive models are incrementally non-linear. Note that the distinction between loading and unloading is unimportant for the hypoplastic constitutive equation, since the non-linear part is always active for both loading and unloading. As a matter of fact, the determination of the yield surface for granular materials is usually rather subjective, since the stress-strain curves generally do not show a clear yielding point as many metallic materials do.¹⁸

To facilitate numerical implementation in a finite element code, constitutive equation (10) can be recast in the following matrix form:

$$\{\dot{\sigma}\} = [L]\{\dot{\epsilon}\} - \{N\}\|\dot{\epsilon}\| \quad (15)$$

where $[L]$ is 6×6 matrix and $\{\dot{\sigma}\}$, $\{\dot{\epsilon}\}$ and $\{N\}$ are 6×1 matrices.

2.3. Failure surface and flow rule

As we know, granular materials fail under increasing shear deformation, i.e. the shear strength is exhausted. The term failure is defined within the framework of hypoplasticity as follows.

A material element is said to be at failure if, for a given stress σ , there exists a strain rate $\dot{\epsilon} \neq 0$ such that the stress rate vanishes, i.e.

$$\dot{\sigma} = H(\sigma, \dot{\epsilon}) = 0 \quad (16)$$

If the total set of stress $\sigma \in \{\sigma | \dot{\sigma} = 0\}$ forms a surface in the stress space, it will be called failure surface. Note that any stress at failure is accompanied by the corresponding strain rate $\dot{\epsilon} \in \{\dot{\epsilon} | \dot{\sigma} = 0\}$, which will be further specified below. Failure is characterized by the pair $(\sigma, \dot{\epsilon})$. Note further that the *critical state* in the Cam-clay model¹⁹ is included in the above definition as a special case for simultaneously vanishing volumetric strain rate, namely $\sigma \in \{\sigma | \dot{\sigma} = 0 \cap \text{tr } \dot{\epsilon} = 0\}$.

Referring to constitutive equation (10), we are now in a position to derive explicit expressions of the failure surface and the flow rule according to the above definition. To facilitate derivation, it is convenient to align the co-ordinates with the principal stress direction. By definition, the stress rate at failure vanishes. That is

$$\{\dot{\sigma}\} = [L]\{\dot{\epsilon}\} - \{N\}\|\dot{\epsilon}\| = \{0\} \quad (17)$$

The direction of strain rate at failure can be readily obtained from equation (17):

$$\frac{\{\dot{\epsilon}\}}{\|\dot{\epsilon}\|} = [L]^{-1}\{N\} \quad (18)$$

Equation (18) relates the direction of strain rate to the stress at failure and characterizes the flow rule. Note that (18) should not be confused with the flow rule in elastoplasticity, where only the plastic strain rate is concerned. More detailed treatment of the failure criterion and the flow rule of hypoplastic constitutive equations can be found in a recent work by Wu and Niemunis.²⁴

By making use of the definition of the norm $\|\dot{\epsilon}\|$ we have

$$\frac{\{\dot{\epsilon}\}^T\{\dot{\epsilon}\}}{\|\dot{\epsilon}\|^2} = 1 \quad (19)$$

Substitution of (18) into (19) yields the equation for the failure surface:

$$f(\sigma) = \{N\}^T([L]^T)^{-1}[L]^{-1}\{N\} - 1 = 0 \quad (20)$$

From the above derivations it can be seen that failure concerns two aspects, namely kinematic and dynamic. As a result, there are two equations which follow from the definition of failure. The first one specifies the direction of strain rate at failure and is called the flow rule while the second one concerns the stress and specifies the failure surface. It is worth noting that the failure surface and the flow rule in hypoplasticity can be derived as *by-products* from the constitutive equation, whereas in elastoplasticity they must be prescribed *a priori*, e.g. the Mohr-Coulomb failure

surface and the associated or non-associated flow rule. A further remark is relevant as to whether the flow rule (17), with reference to the failure surface (20), is associated. A perusal of (18) and (20) suggests that the flow rule is non-associated, since in general $\partial f(\{\boldsymbol{\sigma}\})/\partial\{\boldsymbol{\sigma}\} \neq [\mathbf{L}]^{-1}\{\mathbf{N}\}$.

3. A SIMPLE HYPOPLASTIC CONSTITUTIVE MODEL

Bearing in mind that constitutive equation (10) should be homogenous in $\boldsymbol{\sigma}$, we begin with the simplest case in assuming that the tensorial functions \mathbf{L} and \mathbf{N} in (10) are homogeneous of the first order in $\boldsymbol{\sigma}$. Now, we turn our attention to the following specific version of hypoplastic constitutive equation:¹¹

$$\dot{\boldsymbol{\sigma}} = c_1(\text{tr } \boldsymbol{\sigma})\dot{\boldsymbol{\epsilon}} + c_2 \frac{\text{tr}(\boldsymbol{\sigma}\dot{\boldsymbol{\epsilon}})\boldsymbol{\sigma}}{\text{tr } \boldsymbol{\sigma}} + \left(c_3 \frac{\boldsymbol{\sigma}^2}{\text{tr } \boldsymbol{\sigma}} + c_4 \frac{\boldsymbol{\sigma}^{*2}}{\text{tr } \boldsymbol{\sigma}} \right) \|\dot{\boldsymbol{\epsilon}}\| \quad (21)$$

where c_i ($i = 1, \dots, 4$) are dimensionless material parameters. The deviatoric stress tensor $\boldsymbol{\sigma}^*$ in (21) is defined by

$$\boldsymbol{\sigma}^* = \boldsymbol{\sigma} - \frac{1}{3}(\text{tr } \boldsymbol{\sigma})\mathbf{1} \quad (22)$$

Owing to the fact that constitutive equation (21) is homogeneous of the first degree in stress, the predicted behaviour, e.g. tangential stiffness and shear strength, depends linearly on the stress level. Many experimental investigations in the literature indicate that the deviation from the linear dependence on the stress level may become significant, if large variation of the stress level occurs.^{25,26} Nevertheless, the linear dependence on the stress level in (21) can be regarded as a reasonable approximation for small to moderate variation of the stress level.

As compared with the general representation theorem (6) and (7) the coefficients in constitutive equation (21), c_i ($i = 1, \dots, 4$), are independent of the invariants and joint invariants of $\boldsymbol{\sigma}$ and $\dot{\boldsymbol{\epsilon}}$. The constitutive equation is constructed by picking out several items provided by the representation theorem. In doing so, it is unnecessary to employ the entire irreducible integrity bases provided by representation theorem (6). The choice of a feasible constitutive equation relies largely on numerical simulations of various laboratory tests. To this end, the parameters in the constitutive equation chosen must be at first identified. For this purpose, a computer program has been written to identify the material parameters of constitutive equations within the framework of (10). Details of the procedure to identify the material parameters can be found in the recent work by Wu and Bauer.¹³ Here we will focus our attention on the specific constitutive equation (21) and show how the four parameters can be related to some well-established parameters in soil mechanics such as tangent modulus, Poisson ratio and friction angle.

Explicit expressions of the matrices in (15) for constitutive equation (21) are provided in Appendix I. These expressions can be implemented in a finite element program. For details of the implementation and numerical examples, the reader is referred to Sikora.²⁷

3.1. Identification of parameters

Various laboratory tests have been introduced to investigate the mechanical behaviour of soils. We are concerned with the so-called element tests, in which the stress and strain in a specimen can be inferred from the traction and constraints applied on the boundaries of the specimen. To this end, the matrices of $\boldsymbol{\sigma}$, $\dot{\boldsymbol{\epsilon}}$, $\dot{\boldsymbol{\sigma}}$ and $\dot{\boldsymbol{\omega}}$ characterising the laboratory tests are given in Table I. The governing equations for various laboratory tests can be obtained by substituting the corresponding matrices into constitutive equation (21).

Table I. Expressions of stress, strain rate, stress rate and spin tensors for several laboratory tests

	Oedometer test	Triaxial test	Plane strain test	Simple shear test
σ	$\begin{pmatrix} \sigma_1 & 0 & 0 \\ 0 & \sigma_3 & 0 \\ 0 & 0 & \sigma_3 \end{pmatrix}$	$\begin{pmatrix} \sigma_1 & 0 & 0 \\ 0 & \sigma_3 & 0 \\ 0 & 0 & \sigma_3 \end{pmatrix}$	$\begin{pmatrix} \sigma_1 & 0 & 0 \\ 0 & \sigma_2 & 0 \\ 0 & 0 & \sigma_3 \end{pmatrix}$	$\begin{pmatrix} \sigma_{11} & \sigma_{12} & 0 \\ \sigma_{12} & \sigma_{22} & 0 \\ 0 & 0 & \sigma_{33} \end{pmatrix}$
$\dot{\epsilon}$	$\begin{pmatrix} \dot{\epsilon}_1 & 0 & 0 \\ 0 & 0 & 0 \\ 0 & 0 & 0 \end{pmatrix}$	$\begin{pmatrix} \dot{\epsilon}_1 & 0 & 0 \\ 0 & \dot{\epsilon}_3 & 0 \\ 0 & 0 & \dot{\epsilon}_3 \end{pmatrix}$	$\begin{pmatrix} \dot{\epsilon}_1 & 0 & 0 \\ 0 & 0 & 0 \\ 0 & 0 & \dot{\epsilon}_3 \end{pmatrix}$	$\begin{pmatrix} \dot{\epsilon}_{11} & \dot{\epsilon}_{12} & 0 \\ \dot{\epsilon}_{12} & \dot{\epsilon}_{22} & 0 \\ 0 & 0 & 0 \end{pmatrix}$
$\dot{\sigma}$	$\begin{pmatrix} \dot{\sigma}_1 & 0 & 0 \\ 0 & \dot{\sigma}_3 & 0 \\ 0 & 0 & \dot{\sigma}_3 \end{pmatrix}$	$\begin{pmatrix} \dot{\sigma}_1 & 0 & 0 \\ 0 & \dot{\sigma}_3 & 0 \\ 0 & 0 & \dot{\sigma}_3 \end{pmatrix}$	$\begin{pmatrix} \dot{\sigma}_1 & 0 & 0 \\ 0 & \dot{\sigma}_2 & 0 \\ 0 & 0 & \dot{\sigma}_3 \end{pmatrix}$	$\begin{pmatrix} \dot{\sigma}_{11} & \dot{\sigma}_{12} & 0 \\ \dot{\sigma}_{12} & \dot{\sigma}_{22} & 0 \\ 0 & 0 & \dot{\sigma}_{33} \end{pmatrix}$
$\dot{\omega}$	$\begin{pmatrix} 0 & 0 & 0 \\ 0 & 0 & 0 \\ 0 & 0 & 0 \end{pmatrix}$	$\begin{pmatrix} 0 & 0 & 0 \\ 0 & 0 & 0 \\ 0 & 0 & 0 \end{pmatrix}$	$\begin{pmatrix} 0 & 0 & 0 \\ 0 & 0 & 0 \\ 0 & 0 & 0 \end{pmatrix}$	$\begin{pmatrix} 0 & \dot{\omega}_{12} & 0 \\ \dot{\omega}_{21} & 0 & 0 \\ 0 & 0 & 0 \end{pmatrix}$

Among the various kinds of tests in soil mechanics, the most widely used is the triaxial test. Therefore, it is advantageous if the parameters in a constitutive model can be determined from triaxial tests. In what follows, we will show how the four parameters in constitutive equation (21) can be identified with a single triaxial compression test under constant confining pressure.

Let us consider a triaxial test and write out constitutive equation (21) explicitly. By inserting the corresponding matrices in Table II into constitutive equation (21) we obtain the following system of two differential equations:

$$\dot{\sigma}_1 = c_1(\sigma_1 + 2\sigma_3)\dot{\epsilon}_1 + c_2 \frac{\sigma_1 \dot{\epsilon}_1 + 2\sigma_3 \dot{\epsilon}_3}{\sigma_1 + 2\sigma_3} \sigma_1 + \left[c_3 \sigma_1^2 + \frac{4}{9} c_4 (\sigma_1 - \sigma_3)^2 \right] \frac{\sqrt{(\dot{\epsilon}_1^2 + 2\dot{\epsilon}_3^2)}}{\sigma_1 + 2\sigma_3} \quad (23)$$

$$\dot{\sigma}_3 = c_1(\sigma_1 + 2\sigma_3)\dot{\epsilon}_3 + c_2 \frac{\sigma_1 \dot{\epsilon}_1 + 2\sigma_3 \dot{\epsilon}_3}{\sigma_1 + 2\sigma_3} \sigma_3 + \left[c_3 \sigma_3^2 + \frac{1}{9} c_4 (\sigma_1 - \sigma_3)^2 \right] \frac{\sqrt{(\dot{\epsilon}_1^2 + 2\dot{\epsilon}_3^2)}}{\sigma_1 + 2\sigma_3} \quad (24)$$

Taking the four material parameters c_i ($i = 1, \dots, 4$) as unknowns, (23) and (24) are two linear equations. Provided the stress rates ($\dot{\sigma}_1, \dot{\sigma}_3$) and the strain rates ($\dot{\epsilon}_1, \dot{\epsilon}_2$) are known for two arbitrary stress states (σ_1, σ_3), setting these quantities into the above equations we obtain a system of four linear equations. On solving the equation system, the four parameters c_i ($i = 1, \dots, 4$) can be obtained. For solution of the equation system many standard numerical schemes are readily available. In order to relate the four parameters c_i ($i = 1, \dots, 4$) to some well-established parameters in soil mechanics, let us consider two specific stress states. The first stress state is chosen to be hydrostatic ($\sigma_1 = \sigma_2 = \sigma_3$), i.e. before any deviatoric stress is applied, while the second is chosen to be the stress state at failure. Furthermore, we consider a triaxial test under constant confining pressure, namely $\dot{\sigma}_2 = \dot{\sigma}_3 = 0$. With $R = \sigma_1/\sigma_3$ being the stress ratio, the following parameters are introduced: the initial tangent modulus, $E_i = [(\dot{\sigma}_1 - \dot{\sigma}_3)/\dot{\epsilon}_1]_{R=1}$; the

initial Poisson ratio, $v_i = [\dot{\epsilon}_3/\dot{\epsilon}_1]_{R=1}$; the failure stress ratio, $R_f = [\sigma_1/\sigma_3]_{\max}$; and the failure Poisson ratio, $v_f = [\dot{\epsilon}_3/\dot{\epsilon}_1]_{R=R_f}$. With the above notation the four linear equations obtained from (23) and (24) can be written out in the following matrix form:

$$\begin{bmatrix} 3 & \frac{1}{3}(1-2v_i) & -\frac{1}{3}d_i & 0 \\ 9v_i & -(1-2v_i) & d_i & 0 \\ -(2+R_f)^2 & R_f(2v_f-R_f) & R_f^2 d_f & \frac{4}{9}d_f(R_f-1)^2 \\ v_f(2+R_f)^2 & (2v_f-R_f) & d_f & \frac{1}{9}d_f(R_f-1)^2 \end{bmatrix} \begin{Bmatrix} c_1 \\ c_2 \\ c_3 \\ c_4 \end{Bmatrix} = \begin{Bmatrix} \frac{E_i}{\sigma_3} \\ 0 \\ 0 \\ 0 \end{Bmatrix} \quad (25)$$

with $d_i = \sqrt{1+2v_i^2}$ and $d_f = \sqrt{1+2v_f^2}$. Explicit expressions for c_i ($i = 1, \dots, 4$) can be obtained with the help of the symbolic computational program *Mathematica*.²⁸ They are

$$c_1 = \frac{E_i}{3\sigma_3(1+v_i)} \quad (26)$$

$$c_2 = \frac{9d_f v_i (R_f^2 - 4) + d_i (2 + R_f)^2 (1 + 4v_f)}{d_f (1 - 2v_i) (R_f^2 - 4) + d_i (2v_f - R_f) (R_f - 4)} c_1 \quad (27)$$

$$c_3 = \frac{9v_i (2v_f - R_f) (R_f - 4) - (1 - 2v_i) (R_f + 2)^2 (1 + 4v_f)}{d_f (1 - 2v_i) (R_f^2 - 4) + d_i (2v_f - R_f) (R_f - 4)} c_1 \quad (28)$$

$$c_4 = -\frac{9[(R_f^2 v_f + 1)(R_f + 2)^2 c_1 + (R_f - 1)R_f(2v_f - R_f)c_2]}{d_f(R_f - 1)^2(R_f^2 - 4)} \quad (29)$$

As might be expected, c_2 , c_3 and c_4 in (26)–(29) are proportional to c_1 , i.e. to the initial tangent modulus, since constitutive equation (21) is homogeneous of the first order in stress.

It is not unusual in engineering practice that sufficient experimental data are not available to have a refined calibration of the constitutive model. In this case, it is desirable to reduce further the number of parameters to enable a crude calibration. For this purpose, the expressions in (26)–(29) can be further simplified in view of the triaxial compression tests on Karlsruhe sand reported by Hettler and Vardoulakis.²⁹ Starting from a hydrostatic stress state, the radial strain at the initiation of deviatoric loading was found to remain zero, i.e. $v_i = 0$. This experimental finding was also verified by extensive experiments on various granular materials, e.g. wheat, sugar and artificial granulates.¹¹ The general validity of this observation for other granular materials needs to be further investigated. In the case of vanishing initial Poisson ratio, the expressions in (26)–(29) simplify to

$$c_1 = \frac{E_i}{3\sigma_3} \quad (30)$$

$$c_2 = c_3 = \frac{(R_f + 2)^2 (1 + 4v_f)}{d_f (R_f^2 - 4) + (2v_f - R_f) (R_f - 4)} c_1 \quad (31)$$

$$c_4 = -\frac{9(R_f + 2)^2 [R_f^2 d_f v_f + R_f v_f (2v_f - R_f) + d_f + (2v_f - R_f)]}{d_f (R_f - 1)^2 [d_f (R_f^2 - 4) + (2v_f - R_f) (R_f - 4)]} c_1 \quad (32)$$

Normalizing c_2 and c_4 in the above expressions by c_1 , we are left with two independent parameters, c_2/c_1 and c_4/c_1 , which can be determined by the failure stress ratio R_f and the failure Poisson ratio v_f . At this stage, c_1 is left unspecified. The failure stress ratio R_f is related to the

Table II. Material constants for Karlsruhe medium sand

Material constants	c_1	c_2	c_3	c_4
Loose Karlsruhe sand ($D_r = 0.10$)	-69.4	-673.1	-655.9	699.6
Dense Karlsruhe sand ($D_r = 0.95$)	-101.2	-962.1	-877.3	1229.2

friction angle ϕ as follows:

$$\phi = \arcsin\left(\frac{R_f + 1}{R_f - 1}\right) \quad (33)$$

According to (30)–(32) contours of c_2/c_1 and c_4/c_1 are provided in Figures 2(a) and 2(b) for a wide range of the friction angle ϕ and the failure Poisson ratio ν_f . If, however, no experimental data on the failure Poisson ratio are available, ν_f can be roughly estimated with the help of Rowe's³⁰ dilatancy theory, where the dilatancy relations based on extensive experiments on granular materials with different mineral components, e.g. quartz and feldspar, are given. After

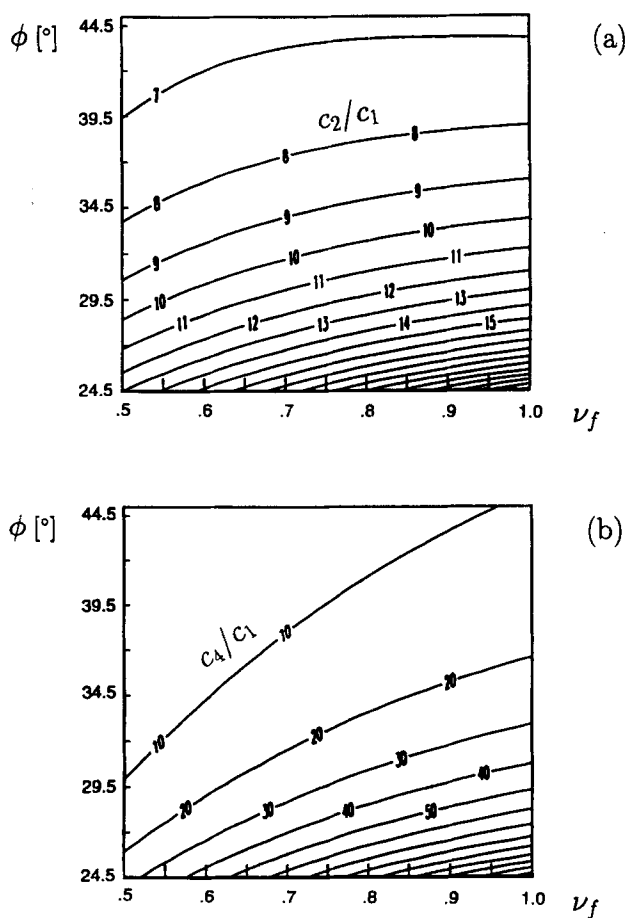


Figure 2. Contours for parameter identification: (a) c_2/c_1 ; (b) c_4/c_1

c_2/c_1 and c_4/c_1 are determined, c_1 can be specified by fitting the initial tangent modulus of a triaxial compression test. The material constants c_i ($i = 1, \dots, 4$) for loose and dense Karlsruhe medium sand are given in Table II.

It should be pointed out that with the help of *Mathematica* the above identification procedure may be easily performed for any constitutive equation within the framework of (10). In addition, the four material parameters can also be identified with other kinds of tests, e.g. the oedometer test³¹ and the plane strain test.³² A combined identification procedure by using experimental data from both triaxial and oedometer tests was shown by Bauer.¹² More refined identification of the parameters might be achieved by optimizing the stress and strain paths to be fitted.

3.2. Failure surface and flow rule

The failure surface and flow rule can be derived for constitutive equation (21) according to (20) and (18). The tedious matrix manipulations in deriving the failure surface are greatly eased by

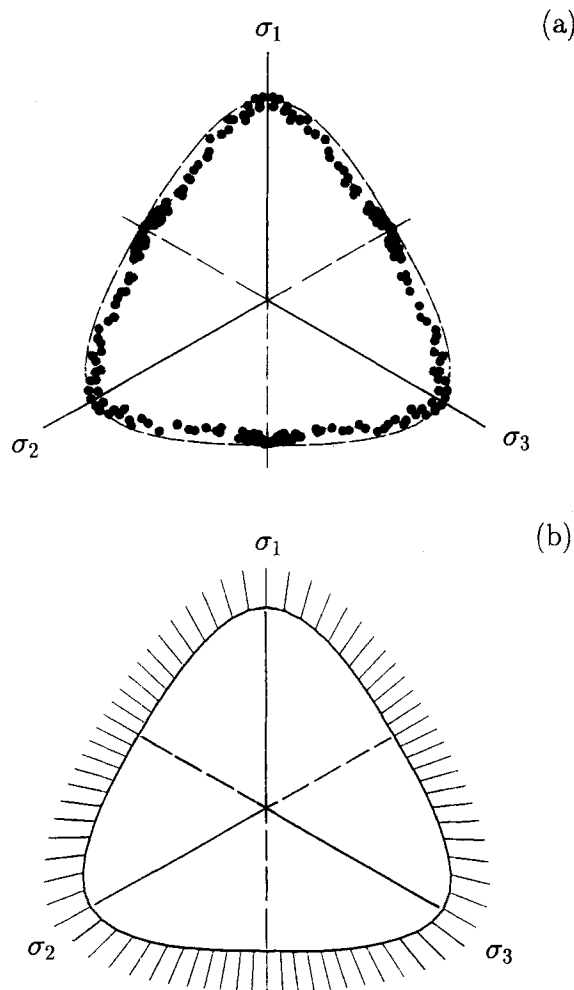


Figure 3. Failure surface and flow rule on an octahedral plane: (a) predicted and experimentally obtained failure surface;³³ (b) direction of strain rate at failure

using the symbolic computational program *Mathematica*. Explicit expressions of the components of $[L]$ and $\{N\}$ can be obtained by setting the shear components of the matrices in Appendix I to zero.

The failure surface calculated from constitutive equation (21) using the constants for dense Karlsruhe sand in Table II are shown on an octahedral plane in Figure 3(a) together with the experimental data by Goldscheider³³ obtained with a true triaxial apparatus. The tested sand is Karlsruhe medium sand, which is composed mainly of quartz with subrounded grains. The index properties and mineral components of Karlsruhe sand can be found in a recent publication by Wu and Kolymbas.³⁴ As compared with the Mohr–Coulomb failure criterion, where the friction angle is assumed to be independent of the intermediate principal stress, the calculated failure surface shows a relatively large influence of the intermediate principal stress. As can be seen from Figure 3(a), the stress at failure away from triaxial compression is slightly over estimated by the constitutive model. This is probably due to the strain localization in the experiments.³⁵ A detailed treatment of strain localization with constitutive equation (21) is beyond the scope of this investigation. It remains to point out that the stress at localized failure is reduced and better agreement can be achieved.³⁶

Since constitutive equation (21) is homogeneous of first order in σ , the tangential stiffness is proportional to the stress level $\text{tr } \sigma$ and the friction angle is independent of it. In principal stress space, the failure surface is a cone with the apex at the origin of the co-ordinate system $(\sigma_1, \sigma_2, \sigma_3)$. The calculated directions of strain rate at failure are shown on an octahedral plane in Figure 3(b) together with the failure surface. A visual inspection of Figure 3(b) suggests that the flow rule is non-associated. This is also in agreement with the well-known fact that the flow rule of granular materials is generally non-associated.

Finally, the effect of the initial density on the failure surface is investigated in Figure 4, where the failure surfaces calculated with the constants for loose and dense Karlsruhe medium sand in Table II are shown on an octahedral plane. It can be seen from Figure 4 that the failure surface for dense sand is more angular than that for loose sand which is in agreement with numerous experimental results in the literature.³⁷

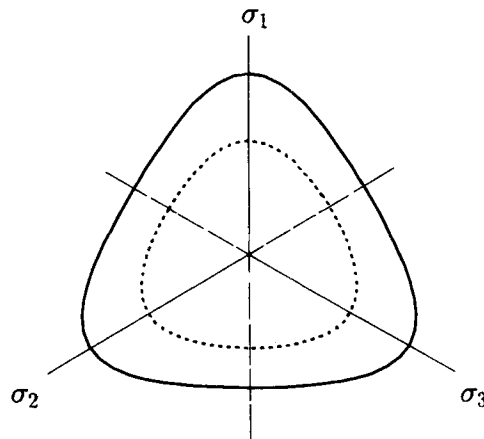


Figure 4. Failure surfaces on an octahedral plane for loose sand (----) and for dense sand (—)

3.3. Performance of the proposed model

Now, we proceed to validate the effectiveness of constitutive equation (21) by simulating several laboratory tests. Explicit expressions for a specific kind of test can be obtained by substituting the corresponding matrices in Table I into constitutive equation (21).

3.3.1. Triaxial tests. The governing differential equations for triaxial tests are (23) and (24). Starting from an initial stress state (σ_1, σ_3) , equations (23) and (24) contain four unknowns, namely $\dot{\sigma}_1, \dot{\sigma}_3, \dot{\epsilon}_1$ and $\dot{\epsilon}_3$. Following a given stress or strain path, two of the four unknowns can be specified. In a restricted sense, the specification of a stress or a strain path is equivalent to the specification of the corresponding boundary condition. Take the conventional triaxial compression test with constant confining pressure for example, we have $\dot{\sigma}_3 = 0$ and $\dot{\epsilon}_1 = -1$, respectively. Note that any positive scalar can serve as the norm of strain rate, since the constitutive equation in concern is rate-independent. In each time step, the radial strain rate is to be calculated from (24). For the solution of (24), any well-established numerical scheme will serve. The radial strain increment obtained in this way will be set into (23) to get the axial stress increment. The stress is then updated to get the initial stress for the next time step. In general, the updating of stress for a time step Δt can be performed as follows:

$$\boldsymbol{\sigma}(t + \Delta t) = \boldsymbol{\sigma}(t) + \int_t^{t+\Delta t} \dot{\boldsymbol{\sigma}}[\boldsymbol{\sigma}(\tau), \dot{\boldsymbol{\epsilon}}(\tau)] d\tau \quad (34)$$

Due to the complexity of the constitutive equation, the above integral can be rarely performed analytically. Therefore, numerical schemes are often resorted to.³⁸ We will not pursue this matter further. In the present paper, a simple one-step, Euler forward scheme is adopted. For more refined integration methods, e.g. the Runge–Kutta method, the reader is referred to Sikora.²⁷

Numerical simulation of triaxial compression tests on loose and dense Karlsruhe sand with a constant confining pressure of $\sigma_3 = 100$ kPa is shown in Figures 5 and 6. Both the numerical simulation and experiment are started from a hydrostatic stress state. It can be seen from the numerical results in Figures 5(a) and 6(a) that the tangential stiffness decreases gradually with axial strain and eventually vanishes at failure. The simulation of loose sand in Figure 5(b) shows that the volume change is contractant and vanishes at failure. The calculated volume change of dense sand in Figure 6(b) is initially contractant and subsequently dilatant. After failure is reached, the volumetric strain increases almost linearly with the axial strain.

The following remark is concerned with the volume change at very large deformation. As may be seen from Figure 6(b), the rate of volume change is constant after failure is reached. For large deformation, however, it would be plausible to assume that the rate of volume change will decrease with the deformation and vanish eventually. Correspondingly, the shear stress will drop to the residual shear strength. This phenomenon is called strain softening. In the laboratory, however, large deformation can be hardly realized without inducing localization in the form of one or more shear bands.³⁹ According to Drescher and Vardoulakis⁴⁰ pronounced strain softening should be attributed to structural or geometrical effect. It remains to point out that the analysis of localized bifurcation with constitutive equation (21) results in reduced shear strength and volume change.³⁶

The behaviour of sand is known to depend on the stress path. The capability of the proposed model to account for the path dependence is demonstrated by simulating the triaxial tests on medium dense Erksak sand.⁴¹ The specimens were first subjected to a hydrostatic stress of 250 kPa. The applied stress paths are depicted in Figure 7. Along paths 1 and 4, the radial stress

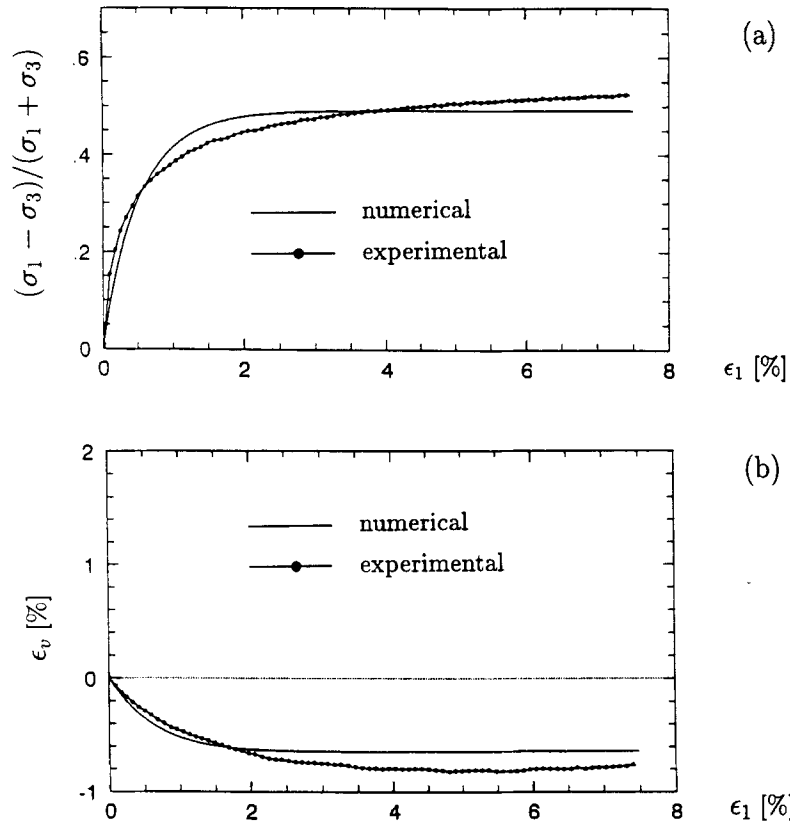


Figure 5. Comparison of numerical and experimental triaxial compression test on loose sand ($\sigma_3 = 100$ kPa): (a) stress ratio vs. axial strain; (b) volumetric strain vs. axial strain

σ_3 and the axial stress σ_1 are kept constant, respectively. Paths 2 and 3 are followed by reducing the radial stress and increasing the axial stress simultaneously. The numerical results are presented in Figure 8 together with the experimental data. The following material constants are used for the numerical simulation: $c_1 = -200.0$, $c_2 = c_3 = -1572.5$, $c_4 = 2583.3$. The variation of both strength (Figure 8(a)) and dilatancy (Figure 8(b)) with stress paths is well described by the constitutive model. The discrepancy between the numerical and experimental results for path 1 is probably due to the relatively large increase of the stress level along path 1.

We now turn our attention to undrained triaxial tests. According to the kinematical constraint, i.e. incompressibility, the constitutive equation can be written as

$$\dot{\boldsymbol{\sigma}} = \mathbf{H}(\boldsymbol{\sigma}, \dot{\boldsymbol{\epsilon}}) + \dot{u}\mathbf{1} \quad (35)$$

The total stress rate $\dot{\boldsymbol{\sigma}}$ in (35) is composed of the sum of the effective stress rate $\mathbf{H}(\boldsymbol{\sigma}, \dot{\boldsymbol{\epsilon}})$, which can be calculated according to constitutive equation (21), and the rate of pore water pressure \dot{u} , which can be obtained from the stress applied on the boundaries. Undrained triaxial compression tests calculated according to constitutive equation (21) are shown in Figures 9(a) and 9(b). The experiments carried out by Castro⁴² are provided in Figures 9(c) and 9(d) for comparison. The material constants used for the numerical simulations are: $c_1 = -20.0$, $c_2 = c_3 = -193.2$,

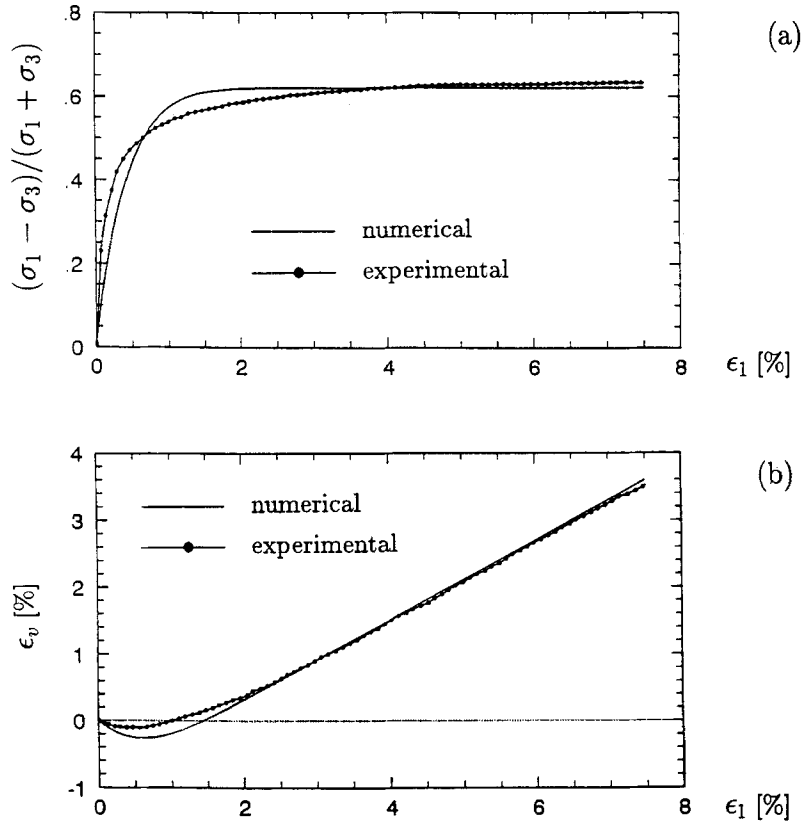


Figure 6. Comparison of numerical and experimental triaxial compression test on dense sand ($\sigma_3 = 100$ kPa): (a) stress ratio vs. axial strain; (b) volumetric strain vs. axial strain

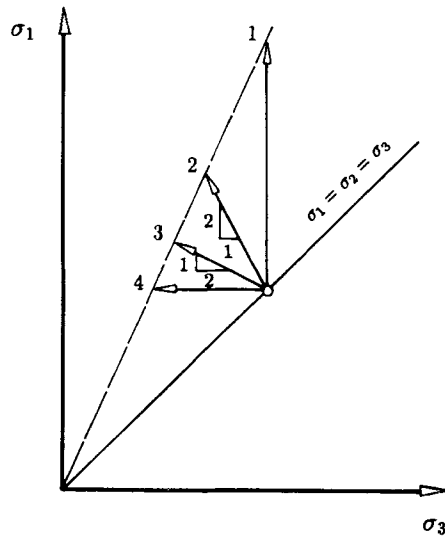


Figure 7. Schematic illustration of the stress paths investigated

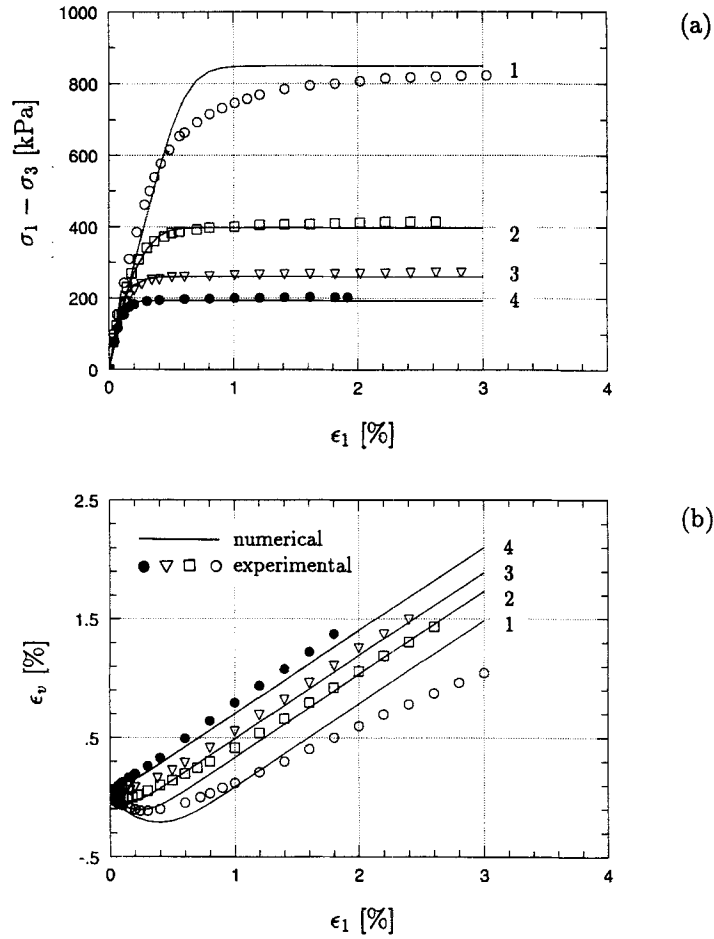


Figure 8. Comparison of numerical and experimental triaxial tests along different stress paths:⁴¹ (a) stress ratio vs. axial strain; (b) volumetric strain vs. axial strain

$c_4 = 190.0$ for loose sand; $c_1 = -33.3$, $c_2 = c_3 = -279.2$, $c_4 = 354.5$ for dense sand. Characteristic stress–strain curves and stress paths of loose and dense sand are well reproduced by the model. Note that the line of phase transition, characterized by the line connecting the origin and the turning point on the stress path, turns out as an outcome of our constitutive model. Comparison between Figure 9(a) and 9(c) shows that the deviatoric stress for loose sand is underestimated by the model. Nevertheless, the numerical results lie on the safe side when the model is used to study liquefaction of loose sand.

3.3.2. *Oedometer tests.* Let us consider the oedometer test with confined radial deformation ($\dot{\epsilon}_3 = 0$). Substitution of the corresponding matrices in Table I into constitutive equation (21) results in the following differential equations:

$$\dot{\sigma}_1 = c_1(\sigma_1 + 2\sigma_3)\dot{\epsilon}_1 + c_2 \frac{\sigma_1 \sigma_1}{\sigma_1 + 2\sigma_3} \dot{\epsilon}_1 + (c_3 \sigma_1^2 + c_4 \sigma_1^{*2}) \frac{|\dot{\epsilon}_1|}{\sigma_1 + 2\sigma_3} \quad (36)$$

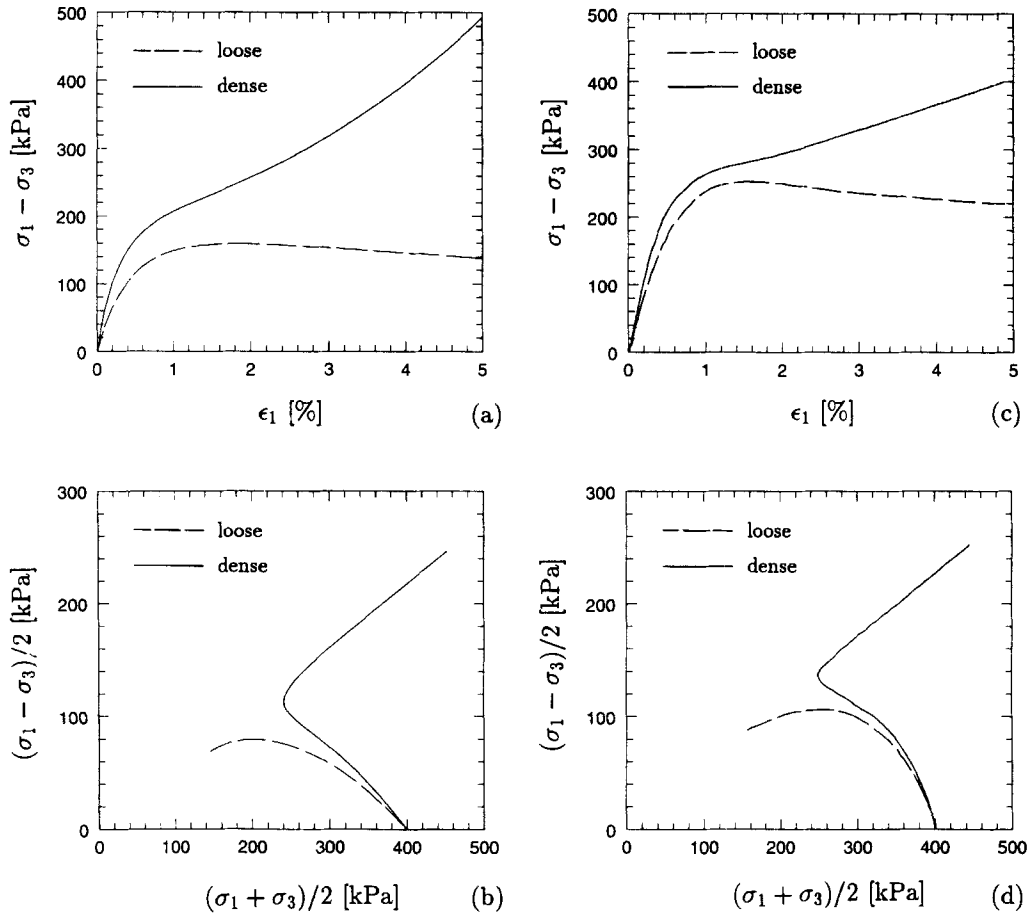


Figure 9. Numerical and experimental undrained triaxial tests:⁴² (a) and (c) deviatoric stress vs. axial strain; (b) and (d) effective stress paths

$$\dot{\sigma}_3 = c_2 \frac{\sigma_1 \sigma_3}{\sigma_1 + 2\sigma_3} \dot{\epsilon}_1 + (c_3 \sigma_3^2 + c_4 \sigma_3^{*2}) \frac{|\dot{\epsilon}_1|}{\sigma_1 + 2\sigma_3} \quad (37)$$

The inclination of the stress path $K_0 = \sigma_3/\sigma_1$, called earth pressure coefficient at rest, is important for a variety of engineering problems. Note that the stress path in an oedometer test is proportional and therefore $\dot{\sigma}_3/\dot{\sigma}_1 = K_0$. The following equation containing K_0 can be obtained from (36) and (37) after some algebraic operations:

$$(36c_1 - 4c_4)K_0^3 + (36c_1 + 9c_3 + 9c_4)K_0^2 + (9c_1 - 9c_3 - 6c_4)K_0 + c_4 = 0 \quad (38)$$

Equation (38) indicates that K_0 depends only on the material parameters c_i ($i = 1, \dots, 4$). For the determination of K_0 , however, it is easier to calculate the stress ratio σ_3/σ_1 directly instead of solving the above algebraic equation. It can be readily shown from (36) that the axial tangential stiffness $\dot{\sigma}_1/\dot{\epsilon}_1$ is proportional to the axial stress σ_1 . That is

$$\dot{\sigma}_1/\dot{\epsilon}_1 = \kappa \sigma_1 \quad (39)$$

The proportionality factor κ in (39) is a function of the material parameters c_i ($i = 1, \dots, 4$) and

K_0 :

$$\kappa = \frac{1}{1 + 2K_0} [(1 + 2K_0)^2 c_1 + c_2 - c_3 - \frac{4}{3}(1 - K_0)^2 c_4] \quad (40)$$

Equation (39) can be integrated analytically to give

$$\ln(\sigma_1/\sigma_{01}) = \kappa \ln(e_1 - e_{01}) \quad (41)$$

where σ_{01} and e_{01} stand for the initial stress and the initial strain, respectively. If the axial strain rate $\dot{\epsilon}_1$ is expressed by the rate of void ratio through $\dot{e} = (1 + e)\dot{\epsilon}_1$, we get the following differential equation from (39):

$$\frac{de}{d[\ln(\sigma_1/\sigma_{01})]} = \frac{1 + e}{\kappa} \approx \frac{1 + e_0}{\kappa} = -C_c \quad (42)$$

where C_c is the compression coefficient and e_0 represents the initial void ratio. A noteworthy case is $e \approx e_0$, i.e. when the volume change is negligibly small. In this case, equation (42) is identical with the widely used compression equation in soil mechanics.⁴³

Figures 10 and 11 show the numerical simulations of oedometer tests on loose and dense Karlsruhe sand using the material constants in Table II. The experiments including the first

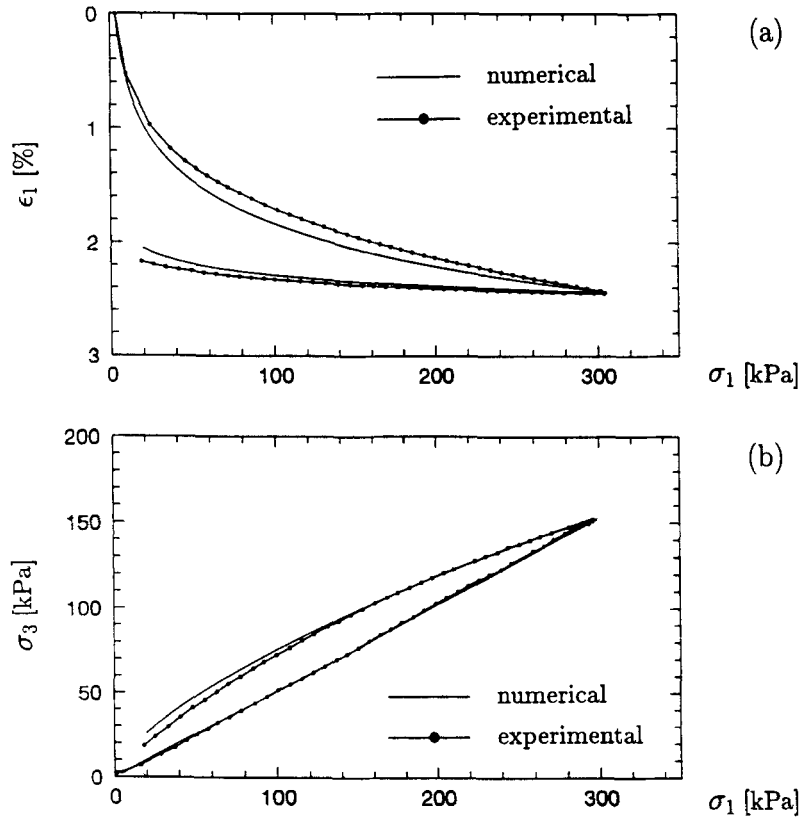


Figure 10. Comparison of numerical and experimental oedometer test on loose sand: (a) axial strain vs. axial stress; (b) radial stress vs. axial stress

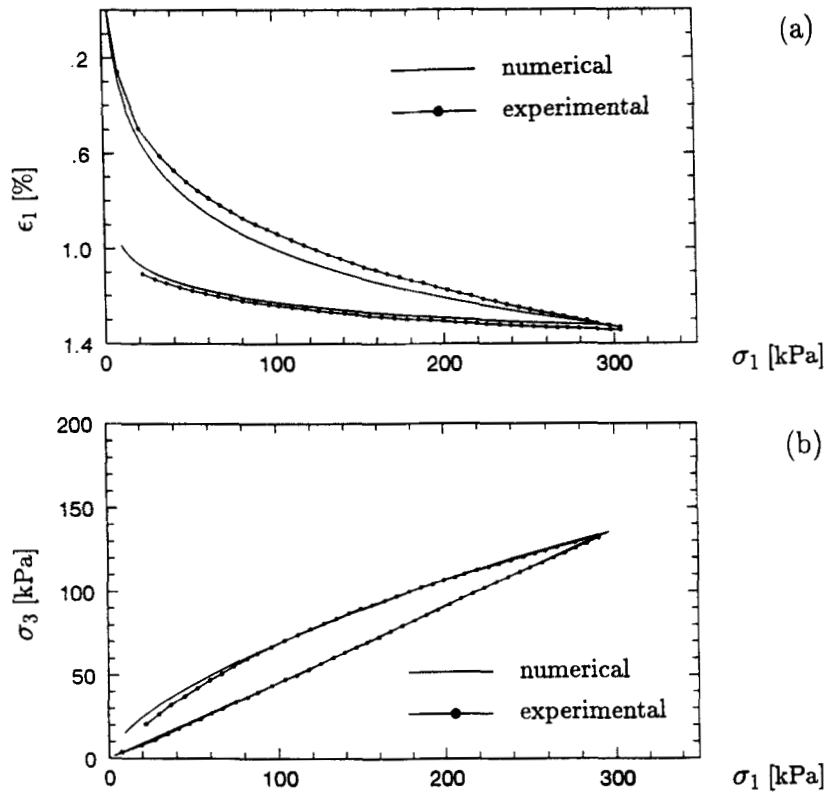


Figure 11. Comparison of numerical and experimental oedometer test on dense sand: (a) axial strain vs. axial stress; (b) radial stress vs. axial stress

loading and the subsequent unloading were performed with specimens of the same densities as the specimens in the triaxial tests in Figures 5 and 6. The stress-strain curves in Figures 10(a) and 11(a) show a gradual increase of the axial tangential stiffness along with the densification. The compressibility of loose sand is much higher than that of dense sand. Also the drastic change of the tangential stiffness from loading to unloading is well described. As may be seen from Figures 10(b) and 11(b), the proportional stress path for the first loading is well reproduced by the model. This implies that K_0 can be regarded as a material parameter. During unloading, the axial stress decreases more rapidly than the radial stress giving rise to an increase of K_0 . This observation is well corroborated by numerous experiments on diverse granular materials.⁴⁴

There are several empirical formulae in the literature to estimate K_0 . The most widely used formula was due to Jaky⁴⁵ by relating K_0 to the friction angle ϕ :

$$K_0 = 1 - \sin \phi \quad (43)$$

The success of using (43) in estimating K_0 has been frequently reported in the literature, e.g. Reference 46. By varying ϕ in triaxial compression, the relation between K_0 and ϕ can be obtained from constitutive equation (21). It will be of interest to compare the predicted relation with the empirical formula (43). In doing so, we assume $\nu_i = 0$. As may be seen from (30)–(32), a further parameter, namely the failure Poisson ratio, needs to be specified. This is furnished by relating the failure Poisson ratio ν_f to the failure stress ratio R_f in analogy to the stress-dilatancy theory due to Rowe.³⁰

In Figure 12, the relation between R_f and ν_f evaluated from triaxial compression tests on Karlsruhe sand after Kolymbas and Wu²⁶ is shown. The experimental data in Figure 12 can be approximated by the following expression:

$$R_f = 8.67\nu_f - 1.20 \quad (44)$$

In this case, it can be seen from (38) that K_0 depends only on the friction angle in triaxial compression. The calculated relation between K_0 and ϕ in triaxial compression is provided in Figure 13 together with the experimental data on Reid Bedford sand.⁴⁷ The tendency that K_0 decreases with increasing ϕ is well reproduced by the constitutive model although K_0 is slightly overestimated for large friction angle.

3.3.3. Simple shear tests. The simple shear test is particularly relevant for modelling field situations where failure is expected to occur along thin shear zones. As was pointed out by Roscoe,⁶ the slip zones are of finite thickness (about ten to 20 times of the mean grain diameter); and within the shear zone the simple shear may be expected to exist. In addition to the practical

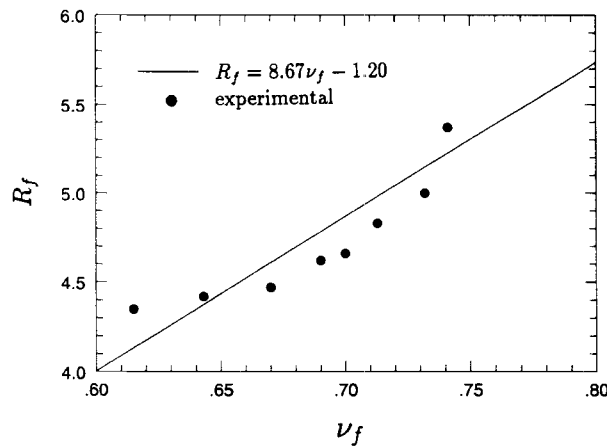


Figure 12. Experimental stress-dilatancy relation

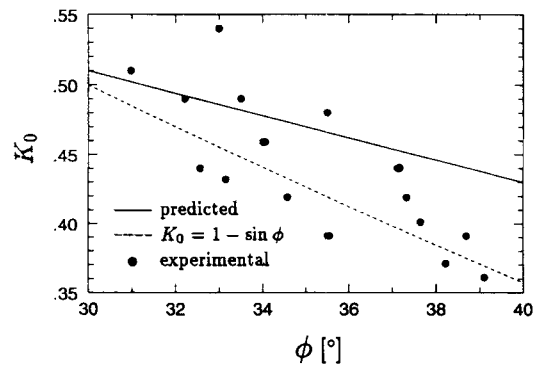


Figure 13. Comparison of predicted, empirical and experimental relation between K_0 and ϕ ⁴⁷

significance, the simple shear test also plays an important role in developing constitutive models. As may be seen from Table I, the spin tensor $\dot{\omega}$ vanishes except for the simple shear test. The simple shear test is one of the few commonly available laboratory tests that permit the application of controlled rotation of the principal axes of stress and strain.

To simulate the simple shear tests numerically, let us consider the motion described by the following expressions:

$$\begin{aligned}x_1 &= X_1 + X_2 f_1(t) \\x_2 &= X_2 + X_2 f_2(t) \\x_3 &= X_3\end{aligned}\quad (45)$$

f_1 and f_2 in (45) represent the shear deformation and the volume change, respectively. For simple shear tests with constant volume (undrained) we have $f_2 = 0$. According to (1) the strain rate and the spin tensors can be obtained from (45):

$$\dot{\epsilon} = \frac{1}{2(1+f_2)} \begin{bmatrix} 0 & \dot{f}_1 & 0 \\ \dot{f}_1 & 2\dot{f}_2 & 0 \\ 0 & 0 & 0 \end{bmatrix}, \quad \dot{\omega} = \frac{1}{2(1+f_2)} \begin{bmatrix} 0 & \dot{f}_1 & 0 \\ -\dot{f}_1 & 0 & 0 \\ 0 & 0 & 0 \end{bmatrix}\quad (46)$$

In performing numerical calculations, the material time rate of stress $\dot{\sigma}$ rather than the Jaumann stress rate $\dot{\sigma}^j$ should be added to the stress in each time step. According to (3) and making use of (46), the relation between $\dot{\sigma}$ and $\dot{\sigma}^j$ can be written out explicitly:

$$\begin{bmatrix} \dot{\sigma}_{11} & \dot{\sigma}_{12} & 0 \\ \dot{\sigma}_{21} & \dot{\sigma}_{22} & 0 \\ 0 & 0 & \dot{\sigma}_{33} \end{bmatrix} = \begin{bmatrix} \dot{\sigma}_{11}^j & \dot{\sigma}_{12}^j & 0 \\ \dot{\sigma}_{21}^j & \dot{\sigma}_{22}^j & 0 \\ 0 & 0 & \dot{\sigma}_{33}^j \end{bmatrix} + \frac{\dot{f}_1}{2(1+f_2)} \begin{bmatrix} 2\sigma_{11} & \sigma_{22} - \sigma_{11} & 0 \\ \sigma_{22} - \sigma_{11} & -\sigma_{12} & 0 \\ 0 & 0 & 0 \end{bmatrix}\quad (47)$$

Again, the governing differential equations for the simple shear test can be obtained by substituting the corresponding matrices in Table I into constitutive equation (21). The following magnitudes are defined for the representation of the results:

The shear angle γ

$$\gamma = \arctan\left(\frac{x_1 - X_1}{x_2}\right) = \arctan\left(\frac{f_1}{1+f_2}\right)\quad (48)$$

The angle between the major principal stress and the horizontal plane χ_σ

$$\chi_\sigma = \frac{1}{2} \arctan\left(\frac{2\sigma_{12}}{\sigma_{11} - \sigma_{22}}\right)\quad (49)$$

The angle between the major principal strain rate and the horizontal plane χ_ϵ

$$\chi_\epsilon = \frac{1}{2} \arctan\left(\frac{2\dot{\epsilon}_{12}}{\dot{\epsilon}_{11} - \dot{\epsilon}_{22}}\right)\quad (50)$$

Numerical simulation of simple shear tests can be performed either under constant normal stress (drained test), i.e. $\dot{\sigma}_{22} = 0$, or under constant volume (undrained test), i.e. $f_2 = 0$. Let us consider the simple shear test under constant normal stress. The procedure of the numerical calculation is similar to that described for the triaxial test and will not be repeated. Numerical simulation of the simple shear test with a constant normal stress of $\sigma_{22} = 98$ kPa reported by

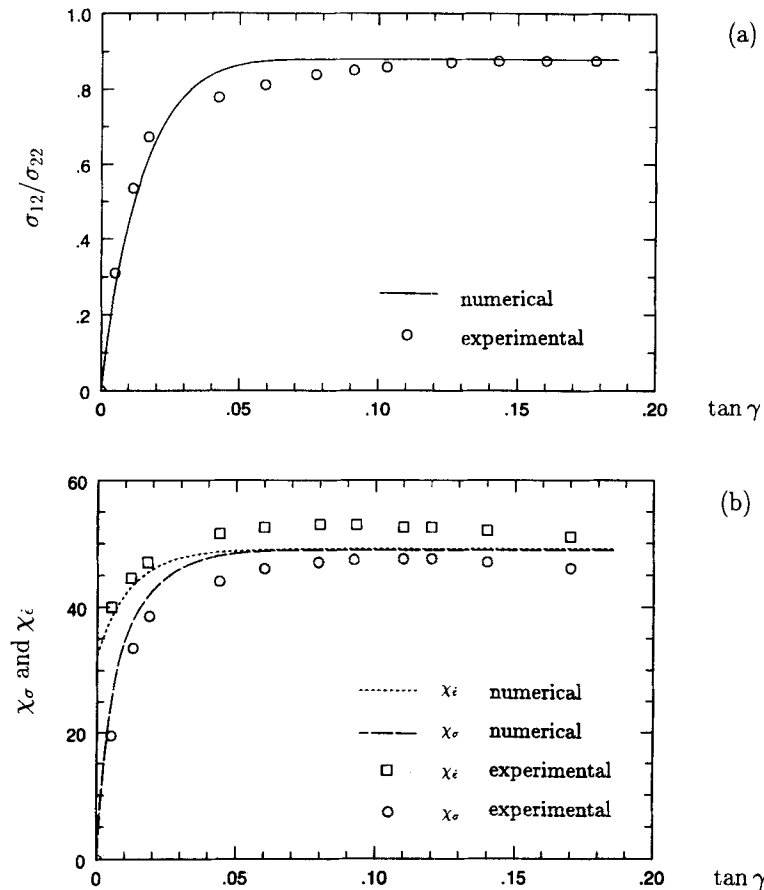


Figure 14. Comparison of numerical and experimental simple shear test;⁴⁸ (a) stress ratio vs. shear angle; (b) χ_σ and χ_ϵ vs. shear angle

Wood *et al.*⁴⁸ is shown in Figure 14. The simulation was performed with the following material constants: $c_1 = -73.3$, $c_2 = c_3 = -542.2$, $c_4 = 719.5$. The test was carried out on dense Leighton Buzzard sand by applying a constant rate of shearing. A gradual transition of the stress-strain curve from the initiation of shearing up to failure can be observed from Figure 14(a).

In most commercially available simple shear apparatus only the normal and shear stress on the horizontal plane, namely σ_{22} and σ_{12} , are measured.⁴⁹ Such apparatus, however, suffer from the drawback that the stress state cannot be fully determined from the measurements. Several attempts have been made to remedy this shortcoming. Roscoe *et al.*⁵⁰ investigated the rotation of the principal stress and the principal strain rate and found out that the principal axes of strain rate and stress coincide in the vicinity of failure. Coaxiality, or coincidence of principal axes of strain rate and stress, may be expressed as $\chi_\sigma = \chi_\epsilon$; its validity provides a possibility to determine fully the stress state. We observe from the numerical results in Figure 14(b) that χ_ϵ is initially much larger than χ_σ . Both χ_σ and χ_ϵ increase with shear straining. In the vicinity of failure, we have $\chi_\sigma \approx \chi_\epsilon$. As may be seen from Figures 14(a) and (14(b)), fairly good agreement between experimental and numerical results is achieved.

In passing, the coaxiality at failure is also within our expectation since the stress and strain rate are related by the isotropic tensorial relation in (18). The significance of coaxiality, which is

a basic assumption in elastoplasticity theory, lies not only in the determination of stress state in experiments but also in developing constitutive models. Again, the coaxiality need not be postulated *a priori* in hypoplasticity. Rather, it is obtained as a consequence of the constitutive model.

Another approach to fully determine the stress state was due to Oda,⁵¹ who related the stress ratio σ_{12}/σ_{22} to the angle χ_σ through the following linear equation:

$$\tan \varphi_{sm} = \sigma_{12}/\sigma_{22} = k \tan \chi_\sigma, \tag{51}$$

in which k is a material parameter. The subscript s and m stand for simple shear and mobilized friction angle respectively. The calculated relation between σ_{12}/σ_{22} and $\tan \chi_\sigma$ is shown in Figure 15 together with the experimental data by Wood *et al.*⁴⁸ Note that the calculated relation, being in good agreement with the experimental data, is non-linear while the relation in (51) is linear. As soon as the angle χ_σ is known, the stress state can be determined by constructing the Mohr's stress circle.

Further, the relation between the friction angle calculated with the principal stresses according to

$$\phi_s = \arcsin \left(\frac{\sigma_1 - \sigma_3}{\sigma_1 + \sigma_3} \right)_{\max} \tag{52}$$

and another angle defined by

$$\varphi_s = \arctan \left(\frac{\sigma_{12}}{\sigma_{22}} \right)_{\max} \tag{53}$$

is considered. ϕ_s is obtained with reference to the plane of maximum stress obliquity whereas φ_s is calculated for the horizontal plane. As we know, the plane of the maximum stress obliquity in the simple shear test does not coincide with the horizontal plane.⁵⁰ In general, ϕ_s is not equal to φ_s . The following empirical relation between ϕ_s and φ_s has been proposed by Stroud:⁵²

$$\tan \phi_s / \tan \varphi_s \approx 1.2 \tag{54}$$

The calculated relation between ϕ_{sm} and φ_{sm} is shown in Figure 16. Note that the calculation is performed from initial shearing until failure, whereas (54) is only evaluated at failure. According to Figure 16 ϕ_{sm} is always larger than φ_{sm} . At failure, we have $\tan \phi_s / \tan \varphi_s \approx 1.4$. The initial stress state was assumed to be a K_0 -state. Initially, we have $\phi_{sm} = \arcsin [(1 - K_0)/(1 + K_0)]$ and $\varphi_{sm} = 0$. This is corroborated by the experimental observation made by Budhu.⁵³

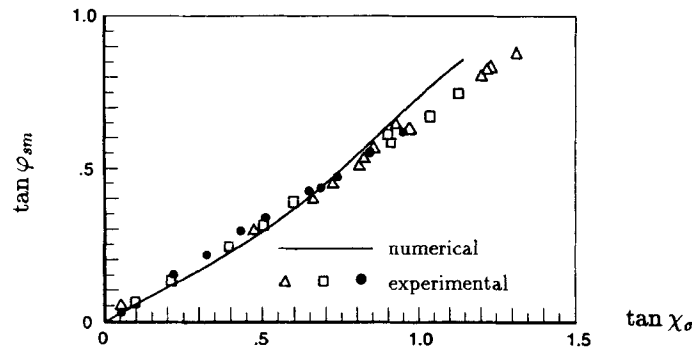


Figure 15. Comparison of predicted and experimental relation between $\tan \varphi_{sm}$ and $\tan \chi_\sigma$ ⁴⁸

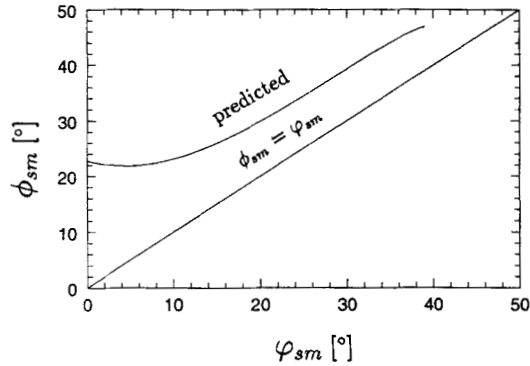


Figure 16. Predicted relation between ϕ_{sm} and φ_{sm}

3.3.4. *Cyclic simple shear tests.* Finally, the capability of the proposed model in describing cyclic behaviour of sand is shown by simulating two simple shear tests under cyclic loading. In doing so, no attempt is made to get the best fitting of the experimental data. Rather, emphasis is placed on qualitative agreement between the predicted and the experimental results.

In Figure 17, the calculated simple shear test under drained condition is compared to the experimental results reported by Pradhan *et al.*⁵⁴ The experiment was carried out on loose Toyoura sand with a constant normal stress of $\sigma_{22} = 100$ kPa. The material constants $c_1 = -123.3$, $c_2 = c_3 = -1162.5$, and $c_4 = -1494.2$ are used to obtain the numerical results.

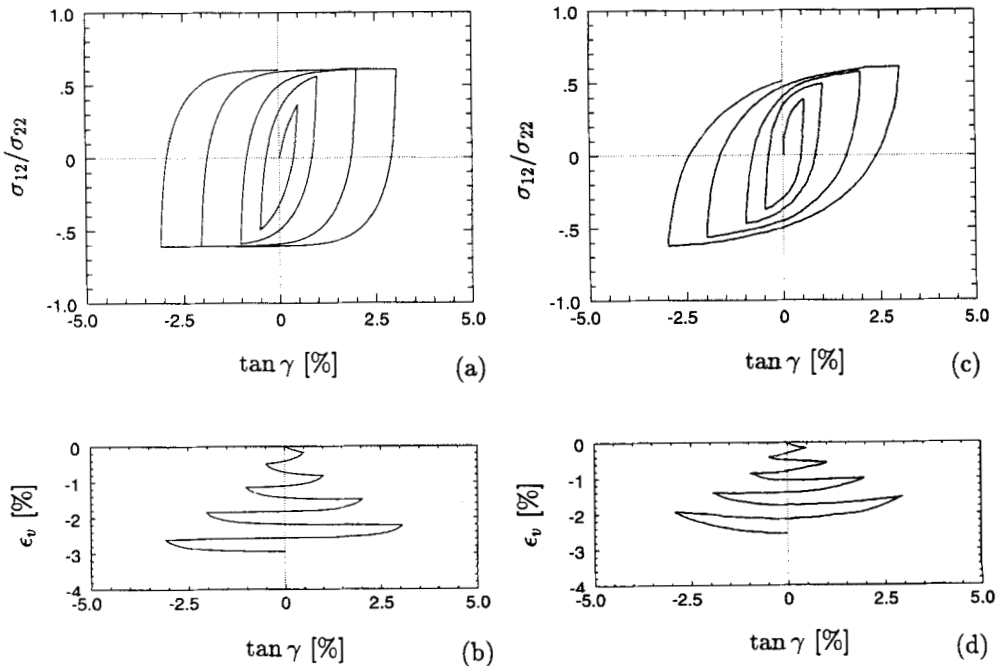


Figure 17. Numerical and experimental simple shear test ($\sigma_{22} = 100$ kPa) after Pradhan *et al.*⁵⁴ (a) and (c) shear stress vs. shear angle; (b) and (d) volumetric strain vs. shear angle

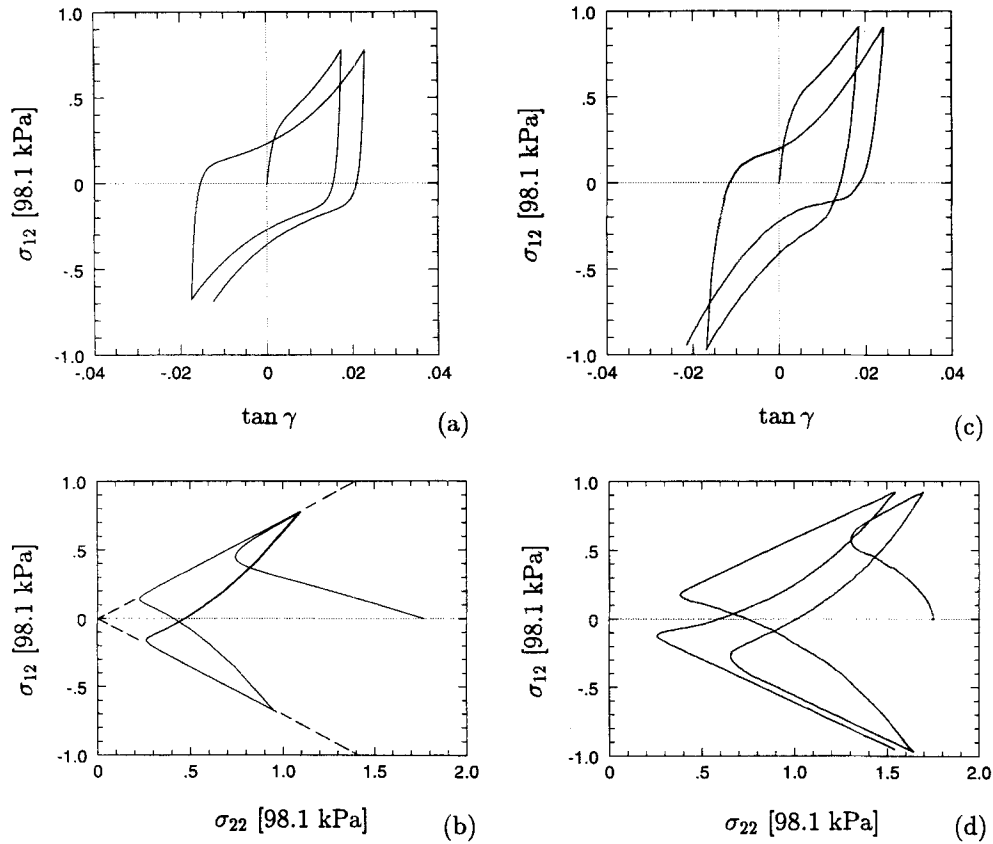


Figure 18. Numerical and experimental simple shear test under undrained condition ($\sigma_{22} = 165$ kPa) after Tatsuoka:⁵⁵ (a) and (c) shear stress vs. shear angle; (b) and (d) effective stress path

The predicted stress–strain curve in Figure 17(a) is somewhat stiffer than the experimental stress–strain curve in Figure 17(c) upon reversal of shearing. Comparison of Figure 17(b) with 17(d) indicates that the densification under cyclic loading is well reproduced by constitutive equation (21).

In Figure 18, numerical results of a simple shear test under undrained condition are presented together with the experimental data reported by Tatsuoka.⁵⁵ The experiment was conducted on dense Toyoura sand with a normal stress of $\sigma_{22} = 165$ kPa. The numerical simulation was carried out with the following material constants: $c_1 = -130.0$, $c_2 = c_3 = -984.9$, and $c_4 = -1374.9$. As may be seen by comparing Figures 18(a) and 18(c), qualitative agreement between the calculated and the experimental stress–strain curve is achieved. The predicted effective stress path in Figure 18(b) shows that both the cyclic mobility and the phase transition manifested in Figure 18(d) is properly reproduced by the proposed model.

4. LIMITATIONS OF THE MODEL

The limitations of the hypoplastic constitutive model reside in the basic assumptions discussed in Section 2. In view of equation (2), the stress rate depends on the instantaneous stress and is independent of the way in which this stress state is reached. As a consequence, the model is not

well suited for complex loading programs involving closed strain cycles. Another limitation that is closely related to equation (2) is that the reduction of the shear strength after failure, so-called strain softening, cannot be obtained. A further limitation lies in the fact that constitutive equation (21) is homogeneous of the first order in stress. The direct consequences are that the tangential stiffness is linearly proportional to the stress level and the friction angle is independent of the stress level. Triaxial tests conducted under elevating confining pressure indicate that both the tangential stiffness and the friction angle decrease with increasing stress level. Therefore, the model should not be applied to engineering problems with large variations of the stress level.

Of course, these limitations may become important for some engineering problems, e.g. for the offshore structures under cyclic loading and in the vicinity of the tip of piles during driving. Nevertheless, the great majority of the problems in geotechnical engineering may be simulated with relatively simple loading programs and with small to moderate change of the stress level, where the model may be applied. In fact, these and other limitations are surmounted in our recent publication¹³ by integrating the critical state into the hypoplastic model. With one set of material constants, the extended model covers a wide range of the stress level and the whole spectrum of initial density from very loose to very dense packing. However, the improvements in the extended model with seven material parameters and three index parameters are gained at the cost of the simplicity of the model. In all, the present paper is an attempt to achieve a compromise between sophistication and simplicity of the model.

5. CONCLUSIONS

It has been shown that the hypoplastic constitutive equation, albeit its simplicity, is capable of capturing the salient features of sand under both drained and undrained conditions. Many well-established concepts in soil mechanics, e.g. failure, flow rule and K_0 , which have to be specified *a priori* in most elastoplastic models, turn out as natural outcomes of the constitutive model. It is the writers' opinion that the utility of a proper constitutive model lies not only in reproducing the experimental results but also in unifying concepts, which might be otherwise regarded as entirely independent.

The proposed constitutive model possesses simple mathematical formulation and contains only four material parameters, which can be related to some widely used parameters in soil mechanics. Rapid identification of the material parameters is made possible by providing two nomographs. To facilitate finite element implementation, explicit expressions in matrix form are provided. The constitutive model presented here opens a new avenue to describe the mechanical behaviour of sand and presents an attractive alternative to the prevailing elastoplastic constitutive models.

ACKNOWLEDGEMENTS

The authors wish to thank Mr. I. Herle from the Czech. Academy of Science for his assistance in producing several figures in the paper. Financial support from the German Research Community (SFB 219-Silos) is gratefully acknowledged. W. W. wishes to thank Lahmeyer International Ltd. for generous support to complete this work.

APPENDIX I: MATRICES $[L]$ AND $\{N\}$ FOR (21)

The fourth-order tensor L and the second-order tensor N in (10) can be written as a 6×6 and a 6×1 matrices, respectively. The constitutive equation can be recast in the following matrix

form:

$$\begin{Bmatrix} \dot{\sigma}_{11} \\ \dot{\sigma}_{22} \\ \dot{\sigma}_{33} \\ \dot{\sigma}_{12} \\ \dot{\sigma}_{13} \\ \dot{\sigma}_{23} \end{Bmatrix} = \begin{bmatrix} L_{11} & L_{12} & L_{13} & L_{14} & L_{15} & L_{16} \\ L_{21} & L_{22} & L_{23} & L_{24} & L_{25} & L_{26} \\ L_{31} & L_{32} & L_{33} & L_{34} & L_{35} & L_{36} \\ L_{41} & L_{42} & L_{43} & L_{44} & L_{45} & L_{46} \\ L_{51} & L_{52} & L_{53} & L_{54} & L_{55} & L_{56} \\ L_{61} & L_{62} & L_{63} & L_{64} & L_{65} & L_{66} \end{bmatrix} \begin{Bmatrix} \dot{\epsilon}_{11} \\ \dot{\epsilon}_{22} \\ \dot{\epsilon}_{33} \\ \dot{\epsilon}_{12} \\ \dot{\epsilon}_{13} \\ \dot{\epsilon}_{23} \end{Bmatrix} - \begin{Bmatrix} N_{11} \\ N_{22} \\ N_{33} \\ N_{12} \\ N_{13} \\ N_{23} \end{Bmatrix}$$

For constitutive equation (21) the matrix $[L]$ can be easily shown to be symmetric. Therefore, it suffices to provide the independent components for $[L]$:

$$\begin{aligned} L_{11} &= c_2 \frac{\sigma_{11}\sigma_{11}}{p} + c_1 p, & L_{12} &= c_2 \frac{\sigma_{11}\sigma_{22}}{p}, & L_{13} &= c_2 \frac{\sigma_{11}\sigma_{33}}{p} \\ L_{14} &= 2c_2 \frac{\sigma_{11}\sigma_{12}}{p}, & L_{15} &= 2c_2 \frac{\sigma_{11}\sigma_{23}}{p}, & L_{16} &= 2c_2 \frac{\sigma_{11}\sigma_{23}}{p} \\ L_{22} &= c_2 \frac{\sigma_{22}\sigma_{22}}{p} + c_1 p, & L_{23} &= c_2 \frac{\sigma_{22}\sigma_{33}}{p}, & L_{24} &= 2c_2 \frac{\sigma_{12}\sigma_{22}}{p} \\ L_{25} &= 2c_2 \frac{\sigma_{13}\sigma_{22}}{p}, & L_{26} &= 2c_2 \frac{\sigma_{22}\sigma_{23}}{p}, & L_{33} &= c_2 \frac{\sigma_{33}\sigma_{33}}{p} + c_1 p \\ L_{34} &= 2c_2 \frac{\sigma_{12}\sigma_{33}}{p}, & L_{35} &= 2c_2 \frac{\sigma_{13}\sigma_{33}}{p}, & L_{36} &= 2c_2 \frac{\sigma_{23}\sigma_{33}}{p} \\ L_{44} &= 2c_2 \frac{\sigma_{12}\sigma_{12}}{p} + c_1 p, & L_{45} &= 2c_2 \frac{\sigma_{12}\sigma_{13}}{p}, & L_{46} &= 2c_2 \frac{\sigma_{12}\sigma_{23}}{p} \\ L_{55} &= 2c_2 \frac{\sigma_{13}\sigma_{11}}{p} + c_1 p, & L_{56} &= 2c_2 \frac{\sigma_{13}\sigma_{23}}{p}, & L_{66} &= 2c_2 \frac{\sigma_{23}\sigma_{23}}{p} + c_1 p \end{aligned}$$

and for $\{N\}$

$$\begin{aligned} N_1 &= -\frac{\bar{\dot{\epsilon}}}{p} [c_3(\sigma_{11}\sigma_{11} + \sigma_{12}\sigma_{12} + \sigma_{13}\sigma_{13}) + c_4(\sigma_{12}\sigma_{12} + \sigma_{13}\sigma_{13} + \sigma_{11}^*\sigma_{11}^*)] \\ N_2 &= -\frac{\bar{\dot{\epsilon}}}{p} [c_3(\sigma_{12}\sigma_{12} + \sigma_{22}\sigma_{22} + \sigma_{23}\sigma_{23}) + c_4(\sigma_{12}\sigma_{12} + \sigma_{23}\sigma_{23} + \sigma_{22}^*\sigma_{22}^*)] \\ N_3 &= -\frac{\bar{\dot{\epsilon}}}{p} [c_3(\sigma_{13}\sigma_{13} + \sigma_{23}\sigma_{23} + \sigma_{33}\sigma_{33}) + c_4(\sigma_{13}\sigma_{13} + \sigma_{23}\sigma_{23} + \sigma_{33}^*\sigma_{33}^*)] \\ N_4 &= -\frac{\bar{\dot{\epsilon}}}{p} [c_3(\sigma_{11}\sigma_{12} + \sigma_{12}\sigma_{22} + \sigma_{13}\sigma_{23}) + c_4(\sigma_{13}\sigma_{23} + \sigma_{12}\sigma_{11}^* + \sigma_{12}^*\sigma_{22}^*)] \\ N_5 &= -\frac{\bar{\dot{\epsilon}}}{p} [c_3(\sigma_{11}\sigma_{13} + \sigma_{12}\sigma_{23} + \sigma_{13}\sigma_{33}) + c_4(\sigma_{12}\sigma_{23} + \sigma_{13}\sigma_{11}^* + \sigma_{13}^*\sigma_{33}^*)] \\ N_6 &= -\frac{\bar{\dot{\epsilon}}}{p} [c_3(\sigma_{12}\sigma_{13} + \sigma_{22}\sigma_{23} + \sigma_{23}\sigma_{33}) + c_4(\sigma_{12}\sigma_{13} + \sigma_{23}\sigma_{22}^* + \sigma_{23}^*\sigma_{33}^*)] \end{aligned}$$

p and $\bar{\epsilon}$ in the above expressions are defined by

$$p = \sigma_{11} + \sigma_{22} + \sigma_{33}$$

$$\bar{\epsilon} = \sqrt{\dot{\epsilon}_{11}^2 + \dot{\epsilon}_{22}^2 + \dot{\epsilon}_{33}^2 + 2(\dot{\epsilon}_{12}^2 + \dot{\epsilon}_{13}^2 + \dot{\epsilon}_{23}^2)}$$

REFERENCES

1. K. H. Roscoe, A. N. Schofield and C. P. Wroth, 'On the yielding of soils', *Géotechnique*, **8**, 22–52 (1958).
2. P. V. Lade, 'Elasto-plastic stress strain theory for cohesionless soils with curved yield surfaces', *Int. j. solids struct.*, **13**, 1019–1035 (1977).
3. Y. F. Dafalias and L. R. Herrmann, 'Bounding surface formulation of soil plasticity', in G. N. Pande and O. C. Zienkiewicz (eds), *Soil Mechanics—Transient and Cyclic Loads*, Wiley, Chichester, U.K., 1982, pp. 253–282.
4. Z. Mróz and S. Pietruszczak, 'A constitutive model for sand with anisotropic hardening rule', *Int. j. numer. anal. methods geomech.*, **7**, 305–320 (1983).
5. K. C. Valanis and J. F. Peters, 'An endochronic plasticity theory with shear-volumetric coupling rule', *Int. j. numer. anal. methods geomech.*, **15**, 77–102 (1991).
6. K. H. Roscoe, 'The influence of strains in soil mechanics', 10th Rankine Lecture, *Géotechnique*, **20**, 129–170 (1970).
7. D. Kolymbas, 'Eine konstitutive Theorie für Böden und andere körnige Stoffe', *Publication Series of the Institute of Soil Mechanics and Rock Mechanics*, No. 109, Karlsruhe University, 1988.
8. W. Wu and D. Kolymbas, 'Numerical testing of the stability criterion for hypoplastic constitutive equations', *Mech. Mater.*, **9**, 245–253 (1990).
9. D. Kolymbas, 'An outline of hypoplasticity', *Ing. Arch.*, **61**, 143–151 (1991).
10. W. Wu and Z. Sikora, 'Localized bifurcation in hypoplasticity', *Int. J. Eng. Sci.*, **29**, 195–201 (1991).
11. W. Wu, 'Hypoplastizität als mathematisches Modell zum mechanischen Verhalten granularer Stoffe', *Publication Series of the Institute of Soil Mechanics and Rock Mechanics*, No. 129, Karlsruhe University, 1992.
12. E. Bauer, 'Zum mechanischen Verhalten granularer Stoffe unter vorwiegend ödometerischer Beanspruchung', *Publication Series of the Institute of Soil Mechanics and Rock Mechanics*, No. 130, Karlsruhe University, 1992.
13. W. Wu and E. Bauer, 'A hypoplastic model for pyknotropy and barotropy of granular soils', in D. Kolymbas (ed.), *Proc. Int. Workshop Modern Approaches to Plasticity*, Elsevier, Amsterdam, 1993, pp. 225–245.
14. C. Truesdell, 'Hypoelasticity', *J. Rat. Mech. Anal.*, **4**, 83–133 (1955).
15. R. Hill, 'Some basic principles in the mechanics of solids without a natural time', *J. Mech. Phys. Solids*, **7**, 209–225 (1959).
16. C. Truesdell and W. Noll, 'The nonlinear field theories of mechanics', in S. Flügge (ed.), *Encyclopedia of Physics III/1*, Springer, Berlin, 1965.
17. C. C. Wang, 'A new representation theorem for isotropic functions, parts I and II', *J. Rat. Mech. Anal.*, **36**, 166–223 (1970).
18. M. Goldschieder, 'True triaxial tests on dense sand', in G. Gudehus, F. Darve and I. Vardoulakis (eds), *Proc. Int. Workshop Constitutive Relations for Soils*, Balkema, Holland, 1982, pp. 11–54.
19. A. N. Schofield and C. P. Wroth, *Critical State Soil Mechanics*, McGraw-Hill, London, 1968.
20. A. Stutz, 'Comportment elasto-plastique des milieux granularie', in A. Sawczuk (ed.), *Foundation of Plasticity*, Noordoff, Leyden, 1973, pp. 33–49.
21. M. A. Romano, 'A continuum theory for granular media with a critical state', *Arch. Mech.*, **20**, 1011–1028 (1974).
22. R. O. Davis and G. Mullenger, 'A rate-type constitutive model for soils with a critical state', *Int. j. numer. anal. methods geomech.*, **2**, 255–282 (1978).
23. G. Gudehus, 'A comparison of some constitutive laws for soils under radially symmetric loading and unloading', in W. Wittke (ed.), *Proc. 3rd Int. Conf. Numer. Methods Geomech.*, Balkema, Holland, 1979, pp. 1309–1323.
24. W. Wu and Niemunis, A. 'Failure criterion, flow rule and dissipation function derived from hypoplasticity', *Int. j. numer. anal. methods geomech.* (submitted).
25. S. Fukushima and F. Tatsuoka, 'Strength and deformation characteristics of saturated sand at extremely low pressures', *Soils Foundations*, **24**, 30–48 (1984).
26. D. Kolymbas and W. Wu, 'Recent results of triaxial tests with granular materials', *Powder Technol.*, **60**, 99–119 (1990).
27. Z. Sikora, 'Hypoplastic flow of granular materials', *Publication Series of the Institute of Soil Mechanics and Rock Mechanics*, No. 123, Karlsruhe University, 1992.
28. S. Wolfram, *Mathematica, a system for doing mathematics by computer*, 2nd ed., Addison-Wesley Publishing Company, Inc., USA, 1991.
29. A. Hettler and I. Vardoulakis, 'Behaviour of dry sand tested in a large triaxial apparatus', *Géotechnique*, **34**, 183–197 (1984).
30. P. W. Rowe, 'The stress–dilatancy relation for static equilibrium of an assembly of particles in contact', *Proc. Royal Soc. A*, **264**, 500–527 (1962).
31. D. Kolymbas and E. Bauer, 'Soft oedometer—a new testing device and its application for the calibration of hypoplastic constitutive laws', *ASTM Geotech. Testing J.*, **16**, 263–270 (1993).

32. H. Feise, C. Lyle and M. Nowak, 'Calibration of a hypoplastic model from true biaxial tests', in D. Kolymbas (ed.), *Proc. Int. Workshop Modern Approaches to Plasticity*, Elsevier, Amsterdam, 1993, pp. 259–275.
33. M. Goldscheider, 'Grenzbedingung und Fließregel von Sand', *Mech. Res. Comm.*, **3**, 463–468 (1976).
34. W. Wu and D. Kolymbas, 'On some issues in triaxial extension tests', *ASTM Geotech. Testing J.*, **14**, 276–287 (1991).
35. J. Desrues, J. Lanier and P. Stutz, 'Localization of the deformation in tests on sand samples', *Eng. Fract. Mech.*, **21**, 909–921 (1985).
36. W. Wu and Z. Sikora, 'Localized bifurcation of pressure sensitive dilatant granular materials', *Mech. Res. Comm.*, **19**, 289–299 (1992).
37. P. V. Lade and J. M. Duncan, 'Elastoplastic stress–strain theory for cohesionless soils', *ASCE Geotech Eng.*, **101**, 1037–1053 (1975).
38. W. Wu, 'A unified numerical integration formula for the perfectly plastic von Mises model', *Int. j. numer. methods eng.*, **30**, 491–504 (1990).
39. I. Vardoulakis, 'Shear band inclination and shear modulus of sand in biaxial tests', *Int. j. numer. anal. methods geomech.*, **4**, 103–119 (1980).
40. A. Drescher and I. Vardoulakis, 'Geometric softening in triaxial tests on granular materials', *Géotechnique*, **34**, 291–303 (1982).
41. Y. P. Vaid and S. Sasitharan, 'The strength and dilatancy of sand', *Can. Geotech. J.*, **29**, 522–526 (1992).
42. G. Castro, 'Liquefaction of sand', *Harvard Soil Mechanics Series, No. 81*, Harvard University, U.S.A., 1969.
43. K. Terzaghi and R. B. Peck, *Soil Mechanics in Engineering Practice*, Wiley, New York, 1948.
44. P. W. Mayne and F. H. Kulhawy, K_0 –OCR relationships in soil, *ASCE Geotech. Eng.*, **108**, 851–872 (1982).
45. J. Jaky, 'The coefficient of earth pressure at rest', quoted by A. Kezdi (1972) in *Proc. 5th Eur. Conf. Soil Mech. Foundation Eng.*, Vol. 2, 1944, pp. 105–130.
46. C. C. Ladd, R. Foott, K. Ishihara, F. Schlosser and H. G. Poulos, Stress–deformation and strength characteristics, State of the art report, *Proc. 9th ICSMFE*, Tokyo, Vol. 2, 1977, pp. 421–494.
47. M. M. Al-Hussaini and F. C. Townsend, 'Investigation of K_0 testing in cohesionless soils', *Technical Report S-75-16*, U.S. Army Engineer Waterways Experimental Station, Vicksburg, Mississippi, 1975.
48. D. M. Wood, A. Drescher and M. Budhu, 'On the determination of the stress state in the simple shear apparatus', *ASTM Geotech. Testing J.*, **2**, 211–222 (1979).
49. L. Bjerrum and A. Landva, 'Direct simple shear tests on a Norwegian quick clay', *Géotechnique*, **16**, 1–20 (1966).
50. K. H. Roscoe, R. H. Bassett and E. R. L. Cole, 'Principal axes observed during simple shear of a sand', *Proc. Geotech. Conf. Shear Strength Properties of Natural Soils and Rocks*, Vol. 1, Norwegian Geotechnical Institute, Oslo, 1967, pp. 231–237.
51. M. Oda, 'On the relationship $\tau/\sigma_n = k \tan \psi$ in the simple shear test', *Soils Foundations*, **15**, 35–41 (1975).
52. M. A. Stroud, 'The behaviour of sand at low stress levels in the simple shear apparatus', *Dissertation*, University of Cambridge, 1970.
53. M. Budhu, 'The mechanism of failure under simple shear strain', *Soils Foundations*, **28**, 119–129 (1988).
54. T. B. S. Pradhan, F. Tatsuoka and Y. Sato, 'Experimental stress–dilatancy relations of sand subjected to cyclic loading', *Soils Foundations*, **29**, 45–64 (1989).
55. F. Tatsuoka, 'Some recent developments in triaxial testing systems for cohesionless soils', state of the art, *ASTM, STP 977*, 7–67 (1988).